Geoarchaeological Assessment of Post-earthquake Kasthamandap
Working Paper 2

May 2019

Geo-Archaeological Assessment of Foundation Fills, Kasthamandap, Nepal

Ian A. Simpson[1], Lois Kelly[1], Tim Kinnaird[2] and Callum Graham[3]
Robin Coningham[4], Chris Davis[4], Kosh Acharya[4], Ram Kunwar[5], Nina Mirnig[6]

[1]Biological and Environmental Sciences, University of Stirling, Stirling, Scotland, UK
[2]School of Earth and Environmental Sciences, University of St Andrews, Scotland, UK
[3]Conservation Science, Historic Environment Scotland, Stirling, Scotland, UK
[4]Department of Archaeology, University of Durham, UK
[5]Department of Archaeology, Nepal
[6]Institute of the Cultural and Intellectual History of Asia, Austria

Correspondence: Ian A. Simpson (i.a.simpson@stir.ac.uk)

1: Introduction

On 25th April 2015 at 11.56 the Gorkha earthquake, magnitude 7.8, struck Nepal resulting in widespread devastation, loss of life and disruption of livelihoods in the Kathmandu Valley (Coningham et al., 2015). This human and cultural disaster had far-reaching social consequences and destroyed or substantially damaged the seven sites of the Kathmandu Valley UNESCO World Heritage Sites (WHS). This aspect of the disaster is universally significant as these sites are 'exceptional testimony to the traditional civilisations of the Kathmandu Valley' and contribute significantly to the understanding of South Asian cultural heritage more broadly (UNESCO, 2017). The loss and damage of these sites also has great local significance, as worship in these living monuments is an important part of local daily religious practices in Nepali cultural and fundamental to the lives of thousands.

This working paper contributes to the analyses of monument foundations by assessing the use of soil material as foundation infill for the Kasthamandap monument, located in the central Hanuman Dhoka Durbar Square. During the Gorhka earthquake, the Kasthamandap super-structure collapsed but very little seismic damage to the foundation brickwork was evident. (Coningham et al, 2015).

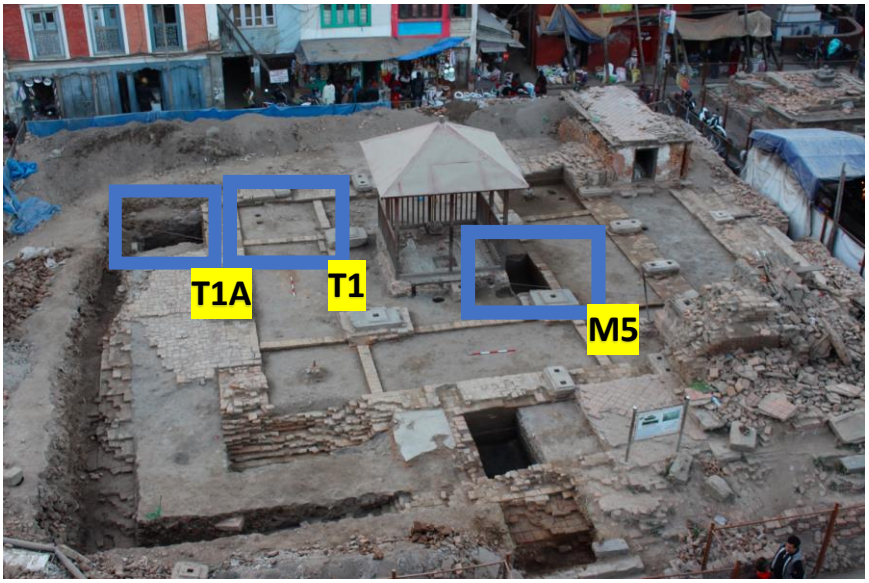

Figure 1. Kasthamandap foundations remain intact post-earthquake despite the destruction of the superstructure. Note that the boxes represent the trench locations with T1 not exposed.

Earthquakes commonly occur in the Kathmandu Valley as it is located in a tectonically active region (Maskey, 2013) with the recent frequency of major historic earthquakes approximately every 60-100 years (NOAA, 2017; Table 1). Furthermore, Hanuman Dhoka Durbar Square is located on ancient lake basin sediments that are soft, unconsolidated and deep. Thus, seismic waves amplify to a very high degree as they move through the sediments. This causes severe vertical movements and vibrations that shake buildings violently during large-scale earthquakes (Maskey, 2013). The varying composition of the sediments in the Kathmandu Valley also results in localised liquefaction creating further structural vulnerability beneath structures (Gautam et al., 2017). These observations suggest that Kasthamandap as a site has likely survived many earthquakes prior to 2015 despite the seismic vulnerability of its location (Maskey, 2013) and opens the question of how foundation fills may

contribute to earthquake proofing of monuments.

Table 1. Past recorded earthquakes in the Kathmandu Valley.

Year (AD)	**1255**	**1833**	**1869**	**1916**	**1934**	**1966**	**1980**	**1988**	**1993**	**2011**	**2015**
Magnitude	7.8	8.0	6.5	7.7	8.0	6.3	6.5	6.6	5.1	5.4	7.8

This paper brings new understanding of the nature of soil materials being utilised within monument foundations and sets these findings in the context of construction methods associated with ritual requirements and earthquake proofing of foundations, an approach not previously been adopted. Currently there is no detailed record of historical constructions or subsequent repairs to Kasthamandap, there are very few documented sources and there are no scientific analyses of its foundations (Coningham et al, 2016). This lack of literature and documentary recording is commonplace in the Kathmandu Valley. As an example, during the 1934 Bihar-Nepal earthquake, the Lamupati monument in Bhaktapur was severely damaged; afterwards, the monument was levelled and sealed below brick paving. No documentation or investigations of the archaeology was conducted and today the only evidence of its existence lies in no more than some paintings, sketches and old photographs (Oldfield, 1860). This type of response to earthquake damage is common in Kathmandu's recent history. (Maskey, 2013; Tiwari, 2017; Weise, 2017) but misses new and fundamental archaeological evidence associated with the foundations.

Currently there is no science-based literature on introduced soils used in early traditional foundations despite the fact that soil or earth materials are commonly used in construction of walls and above ground structures around the world and throughout history. (See for example, Simpson et al., 2006; Parkin & Adderley, 2017; Von der Heide, 2017; Jaquin, 2012; Silveira et al., 2012; Niroumand et al., 2013; Acharya, 2017; Silveira et al., 2012). Despite an extensive search, it was impossible to find reference to the use of *introduced* soil in traditional *foundation* construction. Similarly, scientific research investigating temple foundations is non-existent in the specific case of the Kathmandu Valley. Langenbach (2015) notes that a lack of knowledge of traditional construction techniques is common in countries that have recently experienced a rapid shift in building technologies from traditional to modern materials and methods. The apparent deliberate use of *introduced* soils in the Kasthamandap *foundation* construction presented in this dissertation is the first to record this in the scientific literature.

There are however aspects of foundation design that are accepted as good practice in traditional earthquake resilience design. These measures include: Location on coarse soils to facilitate well-drained ground, far enough from a river with a relatively deep ground water table (Gautam, 2017); stiff or compact soils that will exhibit non-plastic behaviour (Gautam et al., 2017); levelled foundations (Gautam et al., 2016a); simple 'box-like' configurations with symmetry, even length to breadth ratios and perpendicular angles (Langenbach, 2015); central wooden pillars that run from the foundation to the roof (Gautam et al., 2016b) to supply adequate loading flexibility in the event of intense, violent ground shaking but rigid enough to ensure the structure sways as one component to avoid structural failures (Weise, 2017).

Furthermore, there are South Asian textual sources alluding to the ancient, ritualistic process of foundation construction made with reference to the cosmic 'science' of vernacular and monument construction, instructed by Brahmã the creator. The *Mayamata* and *Mãnasãra* date to the 11th century but thought to incorporate earlier material from earlier centuries. The *Brhatsamhitã* originates in the 6th century and is a text for use by astrologers. In South Asia there is a close link between the cosmos, religion and ritual practices and so this text contains specific chapters on building activities which may have had a wide authority. The relationship between these rituals and construction practices in Nepal from the 6th century is, though, not confirmed as these texts have not been studied in detail and the history of their transmission is not clear (Mirnig, 2017). The *Mãnasarã*, translated by Acharya (1994), the *Mayamata* translated by Dagens (1997), and the *Brhatsamhitã (*unconfirmed translator, 1981*)*, describe an elaborate, multi-stage ceremony specific to the type of building being constructed, and which consisted of many ritual components. They detail everything from finding appropriate ground to build on, to how it should be prepared prior to laying the foundations as well as the specific 'ingredients' and steps to be taken in the initial stages of the construction ritual. There is a mandatory mandala grid layout for the foundation design which comprises 81 different 'plots', within 9 larger brick squares (as illustrated from a plan perspective in Figure 2.), that are each individually treated with different 'offerings' to different deities.

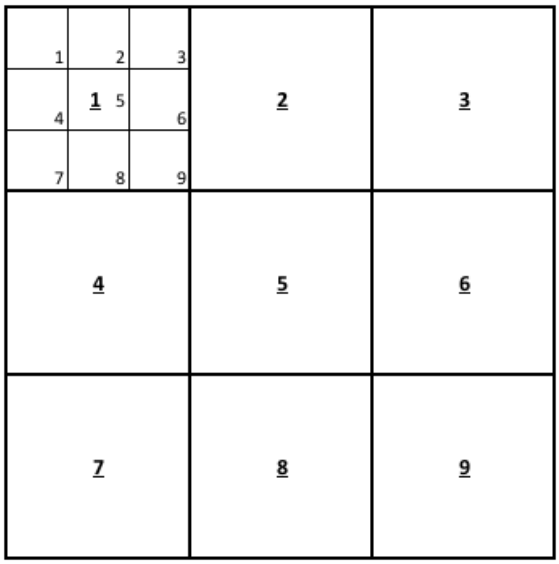

Figure 2. Schematic mandala design foundation, illustrating the 9 brick squares and 81 'plots' within.

There is an exact procedure of laying '7 types of earth' within the foundation walls, followed by different roots and then '8 types of grains'. The laying of the foundation deposit ritual is completed while worshipping with incense, perfumes, rice and flowers, offering food to the gods while chanting. This includes a sacrifice of plants, butter, rice and seeds to the fire, placing pots of water on the deposit and washing the deposit with water and 'the 5 products of the cow' that all must be performed at a specific cosmic moment before the above-surface structural components of the monument can be erected (Dagens, 1997; Acharya, 1994).

These cultural practices are poorly understood in modern day Asia. Today, traditional masons or architects will follow specific designs or rituals for new traditional temple construction that they

were taught by their mentors, but they tend to not know the reasons behind these construction methods or design features as they have been passed down as ancient religious rituals rather than building technology. (Tiwari, 2017). For example, Dixit et al. (2004), notes that elderly craftsmen were encouraged by their grandfathers to incorporate wooden 'ties' carved in the shape of snakes around a building at sill, lintel and floor level in order to protect the structure from evil. This wooden band feature around a building is a common feature in earthquake resistance engineering to ensure walls are protected from out of plane failures during intense shaking.

This paper contributes to initiatives led by UNESCO and the Nepal Department of Archaeology that seeks to protect and rehabilitate post- 2015 earthquake cultural heritage in Nepal. New science-based knowledge of soil use in foundations for early monuments is the primary purpose of the research, deepening understanding not just of Kasthamandap, but also of South Asian temples and vernacular building foundations more generally. It will contribute to the post-earthquake attempts to extend universal value attributes and strive to confirm authenticity of Kasthamandap in keeping with its WHS status. This contribution to the cultural significance of monuments will give a basis for conservation plans and restoration strategies in the future, enabling civil engineers to recognise vitally important elements of heritage value during reconstruction and will directly help to protect and secure the high value cultural heritage of the Kathmandu Valley.

This paper applies geoarchaeological methods to create new narratives of how the foundations of Kasthamandap were constructed with particular attention given to creating new site information from the soils that comprise the infill between the foundations walls. The objectives of the dissertation are to establish the nature of the foundation soils materials at Kasthamandap, characterised as PSD, clay fraction speciation and soil organisation (micromorphology). These data are assessed to determine if there is evidence of deliberate selection and organisation of soil as part of the foundation infill. Explanation of selection and organization evidence are sought in relation to the ritualistic processes detailed in the early Sanskrit texts, and against soil attributes considered to offer a level of earthquake resilience. These objectives will be drawn together in order to explore relationships, if any, between the ritual and earthquake resilient design and may highlight a cultural knowledge of earthquake damage mitigation lost from earlier generations.

2: Methodology

2.1 The Kasthamandap Site

Kasthamandap is located in the centre of Kathmandu at Hanuman Dhoka Durbar Square (Figure 3). It gives Kathmandu its name, situated at the meeting point of four main routes into the ancient city, adjacent to the sacred River Bishnumati. The construction date of Kasthamandap is contested by scholars, but circumstantial evidence suggested a construction date sometime early in twelfth century (Slusser & Vajrãcãrya., 1974). However, recent optically stimulated luminescence dating of samples taken from trench T1, conducted at the SUERC facility has suggested that construction of the monument's foundations was during the seventh century AD (Kinnaird & Simpson, 2016). This sets the construction of Kasthamandap approximately 500 years earlier than previously thought (Coningham et al., 2016). The temple was three-storeys high, made of wood, in Newari style

architecture and it was the biggest of its kind in the Kathmandu valley (Figure 4). Observation of the exposed foundations shows the distinct mandala system of foundation design common in South Asian temples and outlined in the Sanskrit texts. Features include a two-metre deep foundation wall, 9 squares in a grid pattern akin to a Mandala, infilled with soil material. (Slusser & Vajrãcãrya., 1974).

Figure 3. ESRI ArcMap showing location of Kasthamandap in Kathmandu at the centre of four main roads and near the Bishnumati River

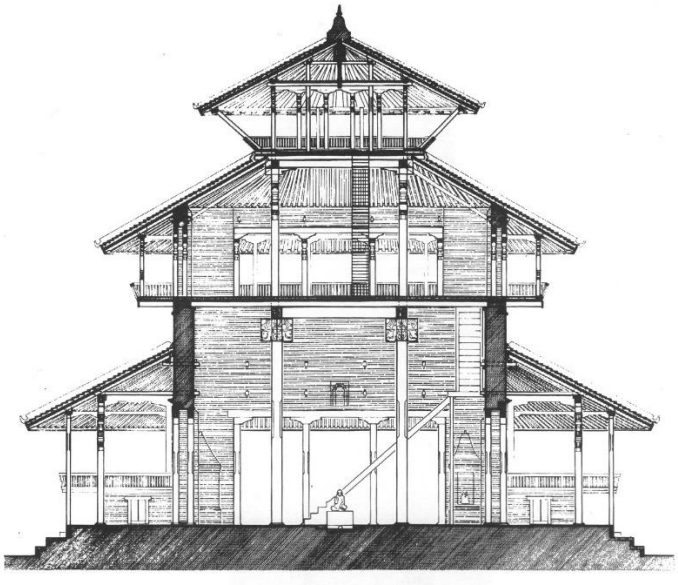

Figure 4. Kasthamandap temple structure, after Slusser & Vajrãcãrya, 1974.

2.2 Field excavation and sampling

Two trenches, T1 and M5, (the locations of which are indicated on Figure 1.) within the monument foundations, were excavated to expose soil profiles. These were formally described, classified and recorded in the field using texture, structure and Munsell colour notation. This allowed a preliminary interpretation of the foundation infill, set a context for the samples taken and was the first step in

building a narrative of the foundation construction. Bulk samples and undisturbed samples in Kubiena tins were systematically collected, recorded and stored from each context within the foundation fills (Figure 5). For trench T1, six samples were collected (357,381,386-393,396-402a, 396-402b & 404-406) and for trench M5, eight soil samples were collected (1222, 1266, 1273, 1275, 1290, 1295, 1298 & 1303). In addition, material from the environmental trench T1A, (from which samples 340 and 339 were used) directly adjacent to the foundations, was collected in the same manner in order to provide a reference to local material.

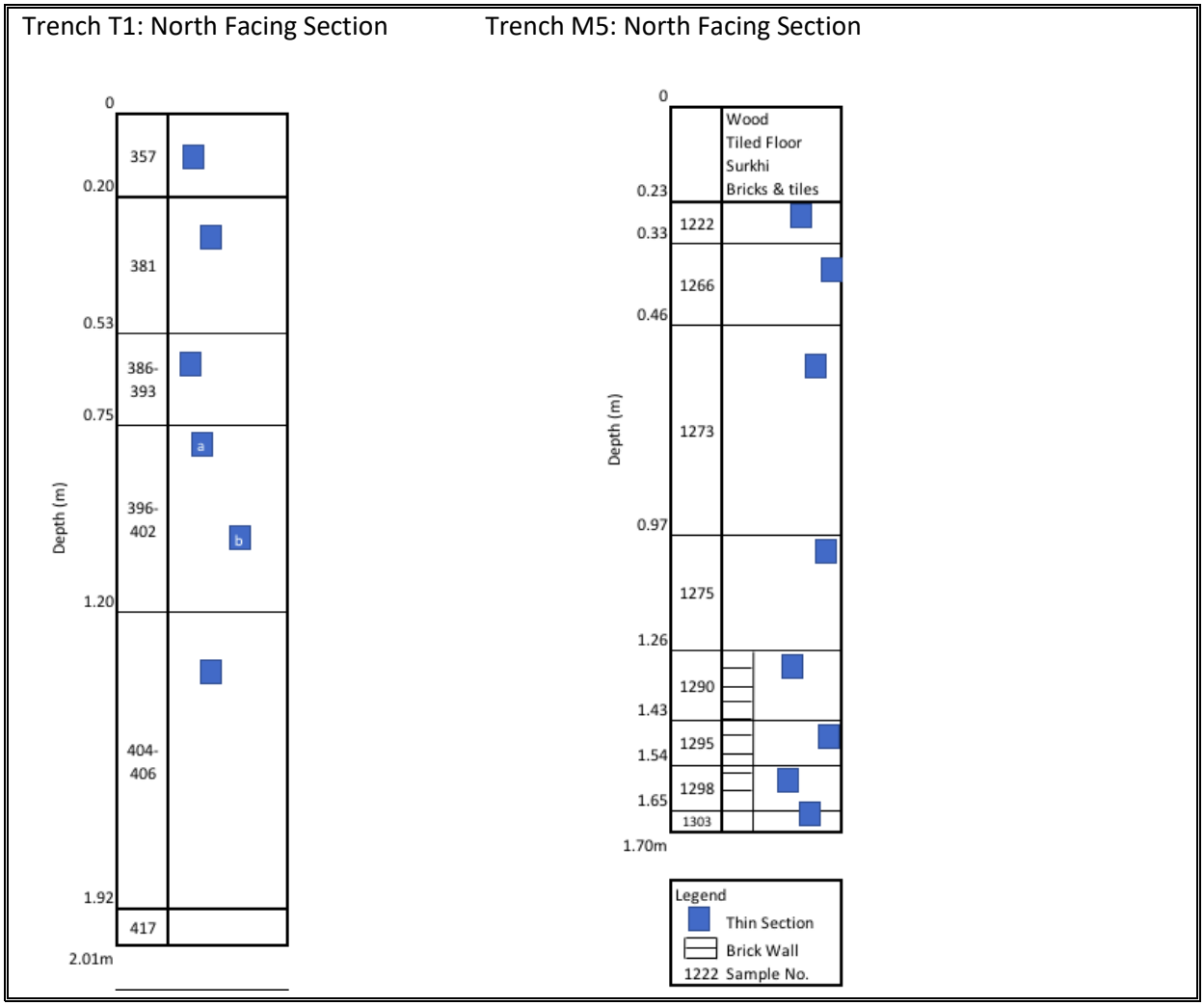

Figure 5. Illustration of the stratigraphic profile of trench T1 and M5 from within the foundation.

2.3 Post-excavation analyses

The sixteen bulk soil samples, one from each context in the 3 trenches, were air dried in foil trays (Figure 6) for 3 days before being separated and homogenized by sieving into <2mm and >2mm fractions. This allowed analyses of the sands, silts and clays separately from the gravels contained in the samples; analyses focussed on the <2mm fraction.

2.3.1 Particle Size Distribution

Samples from the <2mm fraction for each context were prepared for particle size distribution analysis (PSD). A 30ml bottle was filled to the 5ml line with sample material with a spatula. This was then suspended in 15ml of distilled water; 2ml of sodium hexametaphosphate (calgon) was added to aid deflocculation. Samples were agitated overnight by a shaker at low setting for 16 hours. Immediately prior to analysing, each sample was stirred individually on a stirrer plate for a minimum of 20 minutes. This ensured that the suspension was well mixed and homogenous.

Figure 6. Bulk samples from trench T1 and M5 air-drying in foil containers. Note the contrasting colours between samples.

A Coulter Counter; model LS230 was used to undertake PSD analysis of particles from 0.04um to 2000um in diameter. This uses a laser beam to measure the Fraunhofer diffraction pattern of particles giving a flux curve that can be converted to give a proportion of each particle size range within each sample. For particles smaller than 0.4um this machine uses the polarization intensity differential of scattered light (PIDS - rather than laser beams). This system uses six detectors, rotated to measure light scatter intensity at multiple angles for multiple wavelengths to improve the light scatter information and increase accuracy for smaller particles. The Coulter Counter was rinsed for 10 minutes between samples to avoid contamination before the baseline offsets, alignment, background and loading were measured. Samples were dispensed into the column using a pipette until a sufficient loading of 45-55% PIDS was indicated by the LS230 software. A total of five runs of each sample were conducted, and an average taken.

Non-parametric Independent-Samples Median Tests with subsequent post-hoc pairwise comparisons were conducted to quantify the statistical relationships between the PSDs using the median values from the datasets. The non-parametric Mann Whitney test was also used to compare the average medians between the trenches with subsequent pairwise comparisons to identify differences between trench T1 and M5. Statistical analyses were run in IBM SPSS Statistics, Version 23.0.0.3.

2.3.2 X-Ray Diffraction of Clay Extraction

For X-Ray Diffraction (XRD) analyses of the clay (<2µm fraction; Figure 7), sub-samples were taken from the <2mm fraction and initially ground in a pestle and mortar to give a homogenous particle size of ~20um. Following Chipera & Bish (2001), the equivalent of 5ml of this is material was dispensed into a 50ml test tube with a lid, mixed with deionised water to the 40ml mark. This was placed in an ultrasonic bath for 10 minutes to ensure random orientation of the mineral particles and centrifuged at 1000rpm for 3 minutes. This separated out the silts and sands and left the clays in suspension. The clay extraction was pipetted onto a crystallising dish, being careful not to disturb the sediment at the bottom of the test tube and left on a hot plate for approximately 5 hours or until dried out.

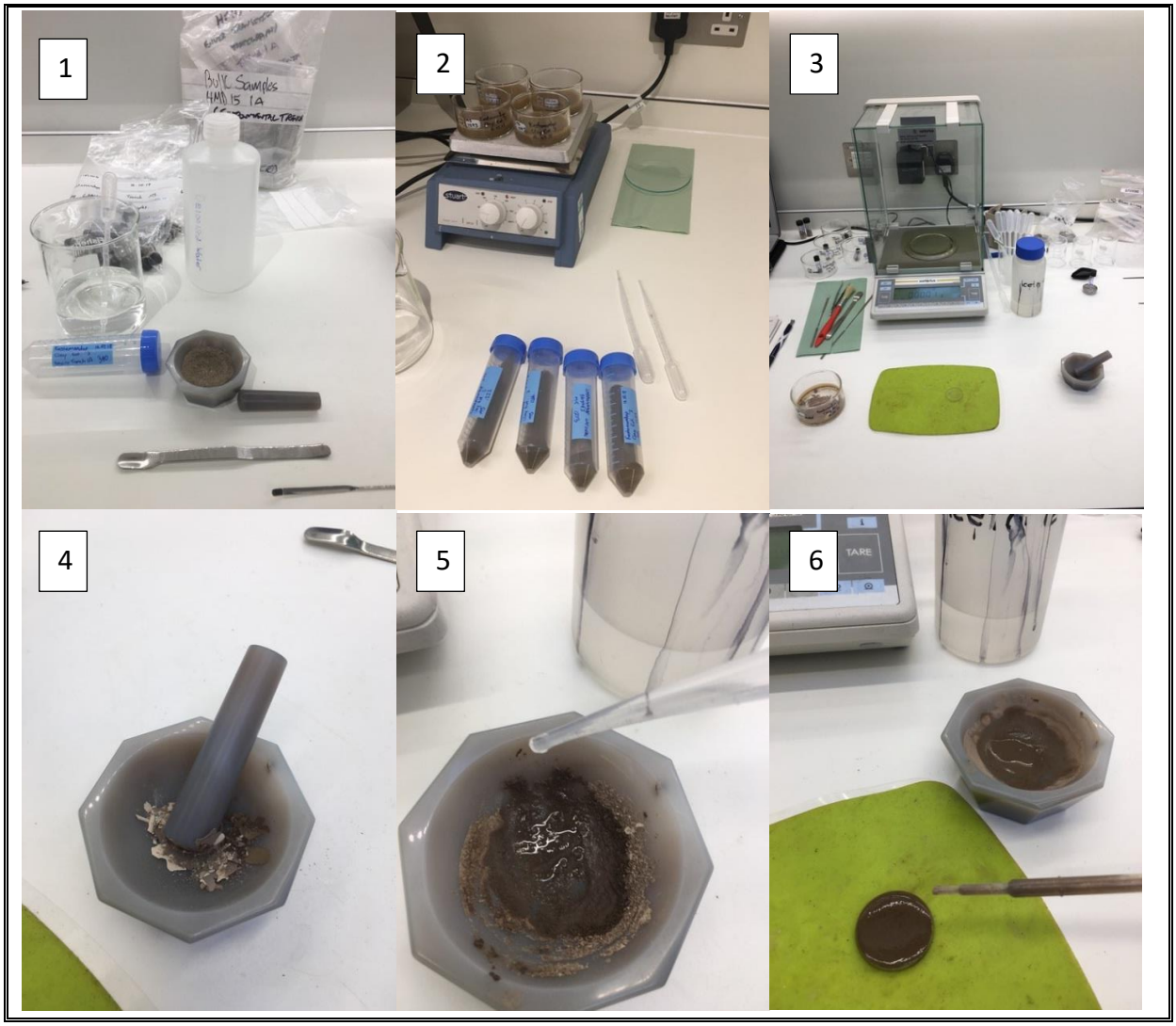

Figure 7. Clay extraction process for the preparation of clay analysis by XRD. ((1). The equipment used to grind and place the sample into solution. (2). The clay extractions drying in their crystallizing dishes after being pipetted out of the test tubes. (3). The equipment used to scrape the dry clays out of the crystallising dishes ready to be prepared for mounting on the glass slides. (4). The clay flakes before grinding and (5). After the addition of acetone to achieve a viscous solution for (6). Pipetting on to the glass slide to achieve a smooth surface.)

The dry clay was scraped from the bottom of the crystallizing dishes with a spatula and brush to be collected in small vials. This was then ground up very gently with a pestle and mortar and

approximately 5-6 drops of acetone to release the clays from their aggregate form. The volume of acetone used is not important, but viscosity is as it has to be transferred by pipette onto a small, circular, zero-background glass slide. It is important that the clay particles do not align in this solution while on the glass slide otherwise they will dry in a preferential orientation. In addition, to this ensuring the sample has a smooth surface when pipetting the clay suspension onto the glass slide keeps background noise to a minimum (ICDD, 2017).

Clay analysis was conducted by X-ray diffraction (XRD) using ARL X'TRA XRD (Figure 8) equipped with a 9-position sample holder, theta-theta goniometer and silicon solid-state detector. This was set to apply CuKα radiation, a voltage of 40kV with a 40mA current. The settings used were 2.0mm divergence and diffracted beam silts, a 2.3 Soller incident beam and a 0.2mm 2.3 Soller slit. This facility, located at the Engine Shed - Historic Environment Scotland - was utilised as they frequently undertake clay analyses for the heritage industry and their experts' knowledge aided in the process from sample preparation through to clay extraction and results collation.

Figure 8. X-ray diffraction machine (ARL X'TRA X-RD) at Historic Environment Scotland Conservation Science Facility.

XRD is used to identify or 'finger print' crystalline materials and in this case was used to determine any compositional (qualitative) differences between the soil samples. Particular attention focused on the clay speciation as this relates to the plasticity of soils under seismic stress. (Chipera & Bish, 2001). X-rays are focussed on a sample from a glass vacuum tube containing an electrode pair. The cathode is heated to release electrons which are drawn across the tube with extreme force to the

metallic anode. When these electrons collide with the atoms, valence electrons are displaced, and high energy x-ray photons are released. A detector moves in a circle around the sample and at each angle from 2-50 2θ, records the number (CPS) of diffracted x-ray photons being scattered by the atomic valence electrons. In order to keep the x-ray beam focused, the sample holder also rotates. (Moore & Reynolds., 1997) Each mineral scatters these photons at different angles (2θ) and so produces a unique diffraction pattern associated with its specific chemical and atomic arrangement; the output is the combination of patterns for each substance present in the soil sample (Zhou et al, 2017). The data was plotted and ThermoElectron software used to determine peak positions. This pattern of peaks was manually and visually compared to the ICDD (2017) international database of diffraction patterns for known crystalline substances.

2.3.3 Micromorphology

Samples collected in Kubiena tins were prepared as thin sections for micromorphological analyses using standard preparation procedures at the University of Stirling (http://www.thin.stir.ac.uk/). Analyses of thin sections was undertaken with an Olympus polarising microscope and described using the standard International System for soil thin section description (Stoops, 2003). Plane polarised light, cross polars and oblique incident light was used. This method allows insight into the architecture of the soil establishing any organisation or arrangement of the soil within the foundation and assess the degree of similarity between the different infill materials. Description and interpretation protocols included working a first working on the sections followed by a second working on the section with an experienced micromorphologist where first descriptions and interpretations were tested to give a final interpretation.

3: Results and Interpretation

3.1 Particle Size Distribution:

3.1.1 M5 Trench

In Trench M5 (Figure 9 and Table 2a, b & c), the samples are very diverse and display unique PSDs indicating that the profile contexts are distinct from each other. Starting with the profile base, 1303 has the lowest median (0.205) and a significantly higher standard deviation (std dev = 1.605) than any of the other samples in either trench. It also has the highest positive skew (1.477) and a positive kurtosis value (0.105) indicating a leptokurtic peak. The distribution is single peaked with a higher percent of coarser particles than fine particles. Sand sized particles made up 53.81% and most of these (32.07%) were very fine sands while there is a significant percent of silts (43.54%) and very low percentage of clays (2.3%).

Sample 1290 contains no medium sands, only 0.17% fine sands and the lowest percent of very fine sands within any sample in this trench at just 8.07%. This is reflected in the low median (0.395) and large standard deviation (0.917) showing a narrow range of particles. This sample has the highest percent of clays at 13.73% but most of the particles (78.02%) are silts. This sample is skewed (0.676)

to the right indicating that the particles are still preferentially coarser than clays and a more negative kurtosis value (-1.041) shows that this distribution is flat and wide.

Sample 1275 also contains coarse sands (5.55%) and it has the highest median (0.725) coupled with a small standard deviation (0.625). This distribution is also dual peaked and has a negative kurtosis value of -0.975 indicating a flatter distribution with a higher percentage of finer particles despite still maintaining a positive skew of 0.529. Sand particles account for 56.99% of this sample with most of them being medium sized (24.36%), while silts make up 38.15% and clays represent only 4.87%.

Sample 1273 is the only other sample that contains coarse sands, but this is minor at 1.91%. The median is high (0.660) and the range of particles sizes represented (Std Dev = 0.777) is comparatively low. The skewness (0.365) is close to normal and the kurtosis (-1.362) is negative indicating a flattened-out distribution. In this sample, silts are the highest percentage particle size (53.1%), fine sands represent 17.53% of the total 40.49% of sands and, clays remain the least represented size at just 6.4%.

Sample 1222 is the only sample in this trench to contain any significant percentage of very coarse sands (3.37%), has the highest percent of coarse sands (11.12%) and has a low percentage of clays (2.69%). It has a median of 0.410 and a greater range of particles sizes than the other samples from M5 (Std Dev = 1.030). 1222 has a high positive skew (1.176) and is one of only two samples with a positive kurtosis value (+0.105).

There is no clear down profile pattern or sorting of material in Trench M5 but rather similar contexts are not adjacent in the sequence but separated by very different material. An Independent-Samples Median Test confirmed that the samples have significantly different medians of percent differential volume. A subsequent pairwise comparison indicated that sample 1303 is most significantly different to samples 1275 (t=13.943, adj. p=0.005) and 1290 (t=11.556, adj. p=0.019).

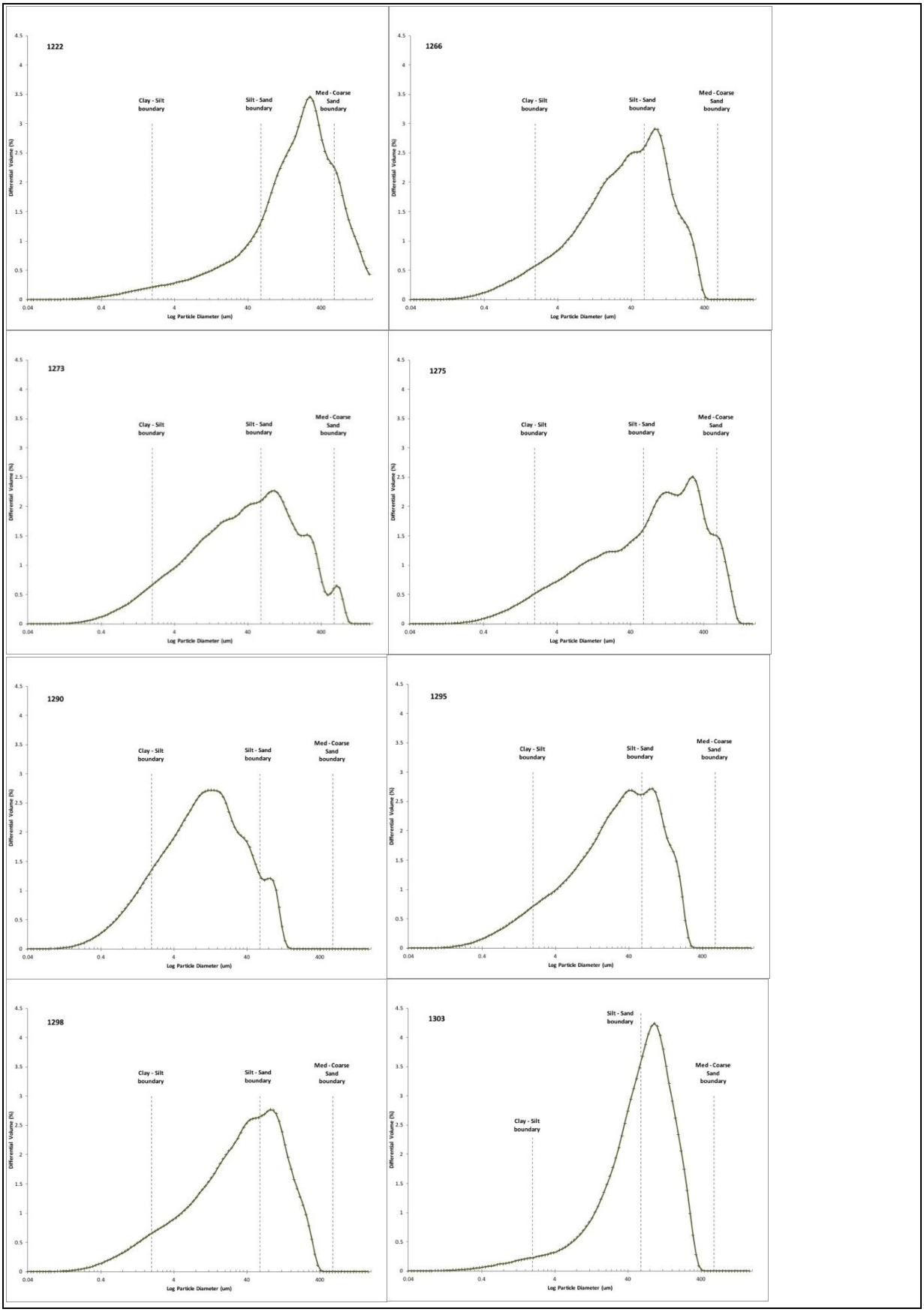

Figure 9. Particle size distributions for trench M5. Note the order of the stratigraphy reads from the top left (1222; top of stratigraphy) to bottom right graph (1303; base of stratigraphy).

Trench M5	Total Clay %	Total Silt %	V. Fine sand %	Fine sand %	Medium sand %	Coarse sand %	V. coarse sand %	Total Sand %
1222	2.3	19.76	14.04	13.38	35.08	11.12	3.37	77.99
1266	5.96	58.02	21.71	8.29	5.96	0	0	35.96
1273	6.4	53.1	17.53	8.63	12.42	1.91	0	40.49
1275	4.87	38.15	16	11.07	24.36	5.55	0.02	56.99
1290	13.73	78.02	8.07	0.17	0	0	0	8.24
1295	7.51	62.78	20.23	7.97	1.56	0	0	29.76
1298	6.9	57.81	21.28	8.86	5.16	0	0	35.3
1303	2.69	43.54	32.07	14.59	7.15	0	0	53.81

Table 2a. % Particle size distributions of trench M5 samples

Table 2b. Statistical PSD descriptors for trench M5 samples.

Trench M5	Median	Standard deviation	Skewness	Kurtosis
1222	0.410	1.015	1.176	+0.105
1266	0.470	0.947	0.788	-0.812
1273	0.660	0.777	0.365	-1.362
1275	0.725	0.790	0.529	-0.975
1290	0.395	0.957	0.676	-1.041
1295	0.460	0.960	0.763	-0.913
1298	0.535	0.934	0.782	-0.802
1303	0.205	1.267	1.477	+0.836

Table 2c. Statistical Analysis and subsequent Pairwise Comparisons of trench M5.

Statistical Analysis	**Samples**	**Test Statistic**	**Sig**	**Adj. Sig.**
Independent-Samples Median Test	M5	1.257	0.016	0.016
Pairwise Comparisons	1303-1275	13.943	<0.001	0.005
	1303-1290	11.556	0.001	0.019
	1303-1298	6.587	0.010	0.288
	1303-1222	5.255	0.022	0.613
	1303-1266	5.255	0.022	0.613
	1303-1273	4.670	0.031	0.859
	1290-1222	4.126	0.042	1.000
	1290-1266	4.126	0.042	1.000
	1275-1222	3.880	0.049	1.000
	1275-1266	3.880	0.049	1.000

There are also subtler statistical differences between sample 1303 and samples 1222 (t=5.255, p=0.022), 1266 (t=5.255, p=0.022), 1273 (t=4.670, p=0.031) and 1298 (t=6.587, p=0.010) that are not considered significant when the Bonferroni adjustment for multiple comparisons is applied. This is also true for samples 1222 and 1266 which each had the same statistical difference to both sample 1275 (t=3.880, p=0.049) and to sample 1290 (t=4.126, p=0.042) prior to the Bonferroni adjustment. The Bonferroni adjustment does overcompensate for multiple comparisons as it multiplies each p value from the pairwise comparison by the number of tests performed.

Samples 1298, 1295 and 1266 are all very similar to each other in nearly every aspect. Medians (0.535, 0.460, 0.470) skewness (0.782, 0.763 & 0.788), kurtosis (-0.802, -0.913 & -0.812) and standard deviations (0.873, 0.922 & 0.897) match closely as the distribution of these samples are all largely the same. The only exception is that 1295 is clearly dual-peaked while the others have less defined broad peaks with shoulders. These samples contain no coarse sands, and mostly silts (57.81%, 62.78% & 58.02%). They all contain ~21% very fine sands and progressively less differential volume as particle size increases (7.97-8.86% fine sands, 1.56-5.96% medium sands). They have slightly higher clay content (5.96-7.51%) than other samples. It is interesting that sample 1266 is so similar but not adjacent to 1298 and 1295 in the soil profile.

3.1.2. T1 Trench

In trench 1 (refer to Figure 10 and Table 4 & 5) there are pairs of samples that are similar to each other. Samples 386-393 and 396-402a are extremely similar in all aspects of their distribution and since they are adjacent to each other in the soil profile, it is highly likely that they are from the same source. Their percent PSDs closely match (sand = 54.81 & 55.11, silt = 39.96 & 39.95, clay = 5.16 & 4.90) down to even the percent distribution of the different sand sizes (very fine = 17.53 &17.75, fine= 11.84 & 11.75, medium = 21.64 & 22.47, coarse = 3.80 & 3.14) and the complete lack of very coarse material. Both have high medians (0.710 & 0.665 respectively), similar standard deviations (0.810 & 0.822), a moderate positive skew (0.621 & 0.587), and a negative kurtosis (-0.816 & -0.938) with low, flat dual peaked distributions.

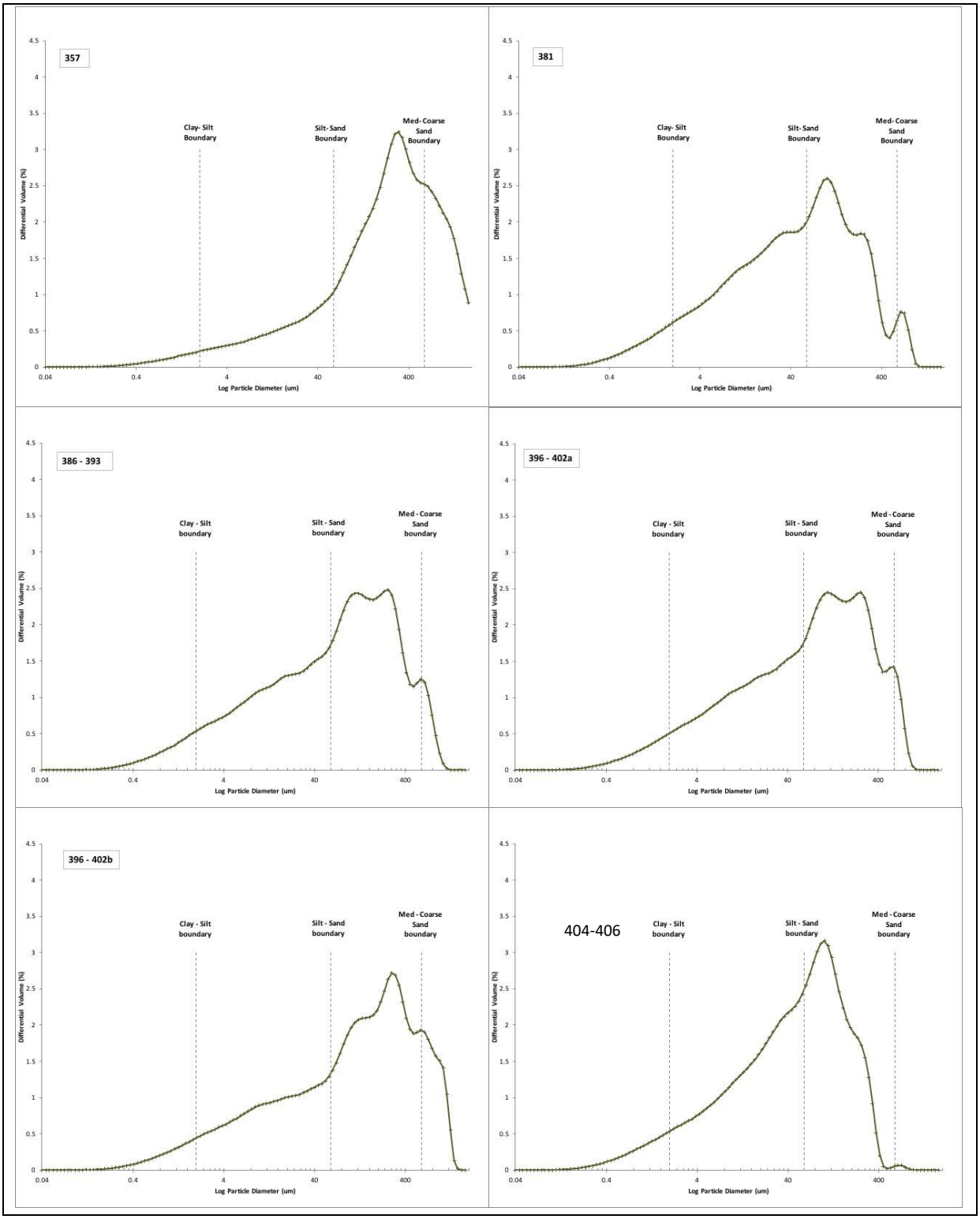

Figure 10. Particle size distributions for trench T1. Note the order of the stratigraphy reads from the top left (357; upper stratigraphy) to bottom right graph (404-406; lower stratigraphy).

Table 3a. % Particle size distributions of trench T1 samples

Trench T1	Total Clay %	Total Silt %	V. Fine Sand %	Fine Sand %	Med Sand %	Coarse Sand %	V. coarse Sand %	Total Sand %
357	2.21	18.45	11.80	11.03	34.36	15.57	6.58	79.34
381	6.29	48.58	19.23	10.03	13.54	2.31	0	45.11
386-393	5.16	39.96	17.53	11.84	21.64	3.80	0	54.81
396-402a	4.90	39.95	17.75	11.75	22.47	3.14	0	55.11
396-402b	4.30	31.92	14.13	10.64	27.44	10.92	0.69	63.82
404-406	5.58	49.37	23.42	11.43	10.03	0.19	0	45.06

Table 3b. PSD Statistical descriptors for trench T1 samples.

Trench T1	Median	Standard deviation	Skewness	Kurtosis
357	0.410	0.963	1.034	-0.306
381	0.645	0.645	0.535	-1.053
386-393	0.710	0.656	0.621	-0.816
396-402a	0.665	0.676	0.587	-0.938
396-402b	0.700	0.645	0.649	-0.761
404-406	0.495	0.907	0.893	-0.459

Samples 357 and 396-402b have similar distributions visually but there are slight difference in the statistics. They have different medians (0.410 & 0.700) and 357 has a higher standard deviation (0.981 & 0.803). 357 is skewed further to the right (1.034) than 396-402b (0.649) which has a more distinct shoulder and a flatter, wider distribution (kurtosis = -0.761). 357 (kurtosis = -0.306) peaks at a higher differential volume.

Samples 381 and 404-406 follow this same trend as they appear relatively similar to each other but differ in a number of statistical respects. The medians differ (0.645 & 0.495 respectively) despite both have almost identical differential volumes of sand (45.11-45.06%), silt (48.58-49.37%) and clay (6.29-5.58%). Neither have any very coarse material but 404-406 has a large range of particle sizes (std dev = 0.952) compared to 381 (std dev = 0.803). 404-406 does have a narrower shape with just a single peak relative to sample 381 which is flatter with a small secondary peak, as reflected by their kurtosis values, -0.459 and -1.053 respectively. Sample 404-406 is also further skewed to the right (0.893) than sample 381 (0.535)

As in trench M5, there is no down profile, preferential sorting of material in trench T1 which would indicate pedogenic processes. 'Pairs' of contexts is evident, but these are separated by a layering arrangement that suggests a deliberate, cultural deposition of these materials. Statistical tests of the means, medians, standard deviations and distributions failed to find any statistically significant differences between the samples in trench T1. However, variations in PSD are subtle and linked to slight variations in the environment that these materials were developed in and so must be considered in a finer detail than these statistical tests allow.

3.1.3 Comparison of trench T1 and M5

When comparing trench M5 to T1 the Mann Whitney test confirmed that both the medians (t=3.593, p=0.650) and distributions (t=2.791, p=0.740) of the particles sizes between M5 and T1 are not significantly different to each other at the 5% significance level. An Independent-Samples Median Test found that at least two samples between the trenches were significantly different to each other (t=26.116, p=0.016) and so a pairwise comparison was then conducted to determine which samples differed. Sample 1303 from trench M5 was significantly different to samples 381 (t=12.979, p=0.029), 396-402b (t=13.943, p=0.017, 386-393 (t=12.054, p=0.047). 1303 was also more subtly different to the other three samples of T1 before the Bonferroni adjustment.

Table 4. Statistical Analysis and subsequent Pairwise Comparisons, for trench T1 and M5.

Statistical Analysis	**Samples**	**Test Statistic**	**Sig**	**Adj. Sig.**
Mann Whitney Test	M5-T1 (medians)	3.593	0.650	0.650
	M5-T1 (distributions)	2.791	0.740	0.740
Independent-Samples Median Test	M5-T1	26.116	0.016	0.016
Pairwise Comparisons	1303-(396-402b)	13.943	<0.001	0.017
	1303-381	12.979	<0.001	0.029
	1303-(386-393)	12.054	0.001	0.047
	1303-(396-402a)	10.303	0.001	0.121
	1303-357	5.874	0.015	1.000
	1303-(404-406)	5.255	0.022	1.000
	357-1275	3.379	0.066	1.000
	357-1290	3.135	0.077	1.000
	1266-(386-393)	3.880	0.049	1.000
	1266-(396-402b)	4.414	0.036	1.000
	1222-(386-393)	3.880	0.049	1.000
	1222-(396-402b)	4.414	0.036	1.000

There are also subtler statistical differences between sample 357 and samples 1275 (t=3.379, p=0.66), 1290(t=3.135, p=0.077), that are not considered significant when the Bonferroni adjustment for multiple comparisons is applied.

This is also true between samples 1266 and 386-393(t=3.880, p=0.049) and 396-402b (t=4.414, p=0.036) and, also between samples 1222 and 386-393(t=3.880, p=0.049), and 396-402b (t=4.414, p=0.036), prior to the Bonferroni adjustment. The Bonferroni adjustment does overcompensate for multiple comparisons as it multiplies each p value from the pairwise comparison by the number of tests performed.

It is clear that sample 357 is very similar to sample 1222 from trench M5 which is also the top most layer of soil infill. They both have comparable differential volumes of each particle size (sand = 79.34%, silt= 18.45% & clay= 2.21) even down to the percent of different sand sizes, while sample 396-402b does not compare so neatly to 1222 or any of the other samples with 63.82% sands, 49.37% silts and 5.58% clays. Sample 381 is similar to sample 1273 from trench M5 with comparable differential particles size volumes and a distinct distribution pattern with the small secondary peak at the medium-coarse sand boundary. Sample 404-406 is similar to samples 1266, 1295 and 1298 from trench M5 in that their distributions follow the same pattern, however they all have individual differential volumes of each particle size.

3.1.4 Comparison of Foundation fill to environmental material

The two dominant field texture classes from the environmental section were analysed for comparison with the foundation materials. In trench T1A (refer to Figure 11 and Table 6 & 7) sample 340 from trench TA has a high percentage of silt (55.25%) while sands only make up 35.91% and clays account for 8.93%. There are no coarse or very coarse sands in this sample and a progressively decreasing frequency of sand particles as coarseness increases. The cut-off of sand sizes is sharp and distinct at 300um after a dual peaked distribution with a positive skew (0.506) This is reflected in the standard deviation (0.737) which indicates a narrower range of particle sizes than 339. The first peak in the distribution is broad and low compared to the narrow, taller peak that follows but overall the distribution is platykurtic (-1.124) This PSD is unlike any of the foundation trench samples and is significantly different from sample 339 (t=3.880, p=0.049) as shown by the Kruskal-Wallis test and pairwise comparison.

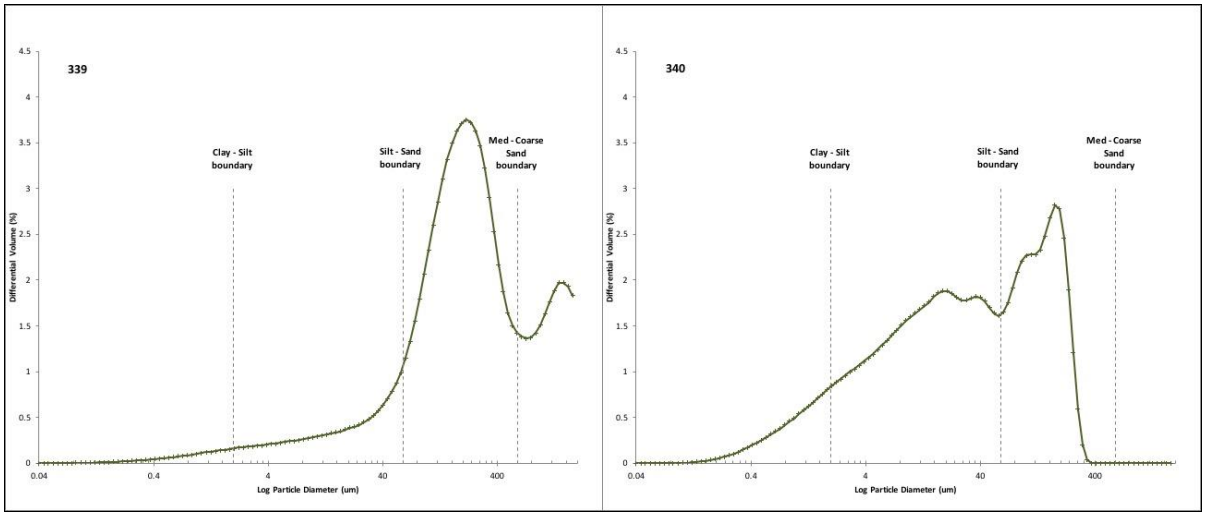

Figure 11. Particle size distributions for trench T1A, environmental control samples.

Sample 339 is dominated sands with only 15.25% of particles not in the sand sized fraction (13.34 silts and 1.91 clays). The majority (31.82%) of these sands are medium, 17.26% are fine and 15.66% are very fine. There is also 10.43% coarse sands and a significant portion of very coarse sands (9.58%) which is a trait that is not reflected in the majority of samples from the either of the trenches within the foundation. The data is skewed (1.324) far to the right and follows a dual-peaked distribution with (0.578) leptokurtic peaks. The range of particle sizes is very wide (Standard deviation = 1.225) and spans the full range of particles sizes from 0.04 to 2000um.

This environmental sample is very similar to sample 1222 from trench M5. They closely follow the same distribution, degree of skewedness and kurtosis with the one exception that 339 is dual peaked. This could suggest that 1222 was taken from the local surroundings but organised in some way that altered the differential volume of coarse material. Sample 339 is also somewhat similar to sample 1303 from trench M5, except that it is further skewed to the right and contains a high percentage of coarse material while 1303 has none. Their peaks both have a similar width and reach comparable differential volumes but 1303 contains far more silt-sized particles.

Table 5a. % Particle size distributions of trench T1A samples

Trench TA	Total Clay %	Total Silt %	V. Fine Sand %	Fine Sand %	Medium Sand %	Coarse Sand %	V. coarse Sand %	Total Sand %
339	1.91	13.34	15.66	17.26	31.82	10.43	9.58	84.75
340	8.93	55.15	16.43	13.09	6.39	0	0	35.91

Table 5b. PSD Statistical descriptors for trench T1A samples.

Trench TA	Median	Standard deviation	Skewness	Kurtosis
339	0.265	1.225	1.324	+0.578
340	0.605	0.737	0.506	-1.124

An Independent-Samples Median Test and subsequent pairwise comparison highlighted that both the medians of trench M5 and T1 were significantly different from that of the environmental trench (M5: t=22.505, p=0.007, T1: t=14.552, p=0.042). Specifically sample 339 was significantly different to sample 1275 (t=9.931, p=0.073) from the M5 trench and sample 396-402b (t=9.931, p=0.046) from the T1 trench. There are also subtler statistical differences between sample 339 and sample 1290 (t=8.698, p=0.003) from the M5 trench and samples 381(t=8.345, p=0.004), 386-393(t=8.345, p=0.004) and 396-402a (t=6.897, p=0.009) from the T1 trench. These differences however are not considered significant after the Bonferroni adjustment for multiple comparisons is applied.

Table 5c. Statistical Analysis and subsequent Pairwise Comparisons, between trenches T1 & M5 and T1A

Statistical Analysis	Samples	Test Statistic	Sig	Adj. Sig.
Independent-Samples Median Test	M5-T1A	22.505	0.007	0.007
	T1-T1A	14.552	0.042	0.042
Pairwise Comparisons	339-396-402b	9.931	0.002	0.046
	339-1275	9.931	0.002	0.073
	339-1290	8.698	0.003	0.143
	339-381	8.345	0.004	0.108
	339-(386-393)	8.345	0.004	0.108
	339-(396-402a)	6.897	0.009	0.242
	339-1298	3.033	0.82	1.000

In summary, the foundation profiles are made up of distinct units which have not been subject to pedogenic processes where we would see particles preferentially sorted down profile. These contexts have been laid down deliberately, in order and a deliberate mixing is evident.
Throughout the profile there is a large degree of variation and each context is unique but there are not high percentages of clays in any. The coarse nature of the material would allow water to drain through the profile. (Gautam, 2017)

Comparison of these samples to the environmental trench indicate that the soil material used for the foundation infill was not collected from the local vicinity. These results strongly suggest not only specific selection of these materials from multiple, non-local sources, but also cultural organisation before deposition in the foundations. A single peaked distribution is uncharacteristic of natural environmental material, suggesting that these contexts were sorted in some way prior to deposition in the foundation.

3.2 X-Ray Diffraction of Clay Extraction

Figures 12 and 13 display results of the XRD analyses and, most prominently, quartz (Qz) is the highest intensity peaks in all samples. Broad, low peaks that correspond to kaolinite and chlorite (Ka), appear in all samples of trench M5 except 1222, 1273 and 1275. All samples of trench T1 except 404-406 also display this peak. Similar peaks that correspond to the signature peak for biotite, muscovite and illite (BMI) at approximately 8-9 2θ, were only detected in samples 1266, 1290, 1295, 1298 and 1303 from the M5 trench. With the exception of 1266, these are the samples from the lower mandala. These minerals are also detected in samples 381 and 396-402b from trench T1 but are shifted to lower peak positions than those in trench M5. These samples are all similar to the composition of the environmental sample 340 (Figure 14). Micas and illite have overlapping signature peaks at multiple positions because they are chemically and structurally similar in that they have a basic arrangement of a central silica octahedral between two tetragonal sheets and contain the same elements in highly variable compositions. The same is true of kaolinite and chlorite which share peak positions and, the quartz signature peak at 27 2θ is shared by many other

minerals. (Zhou et al, 2017). Thus, it is difficult to determine if only one of these mineral mimics is present in these samples without further treatments.

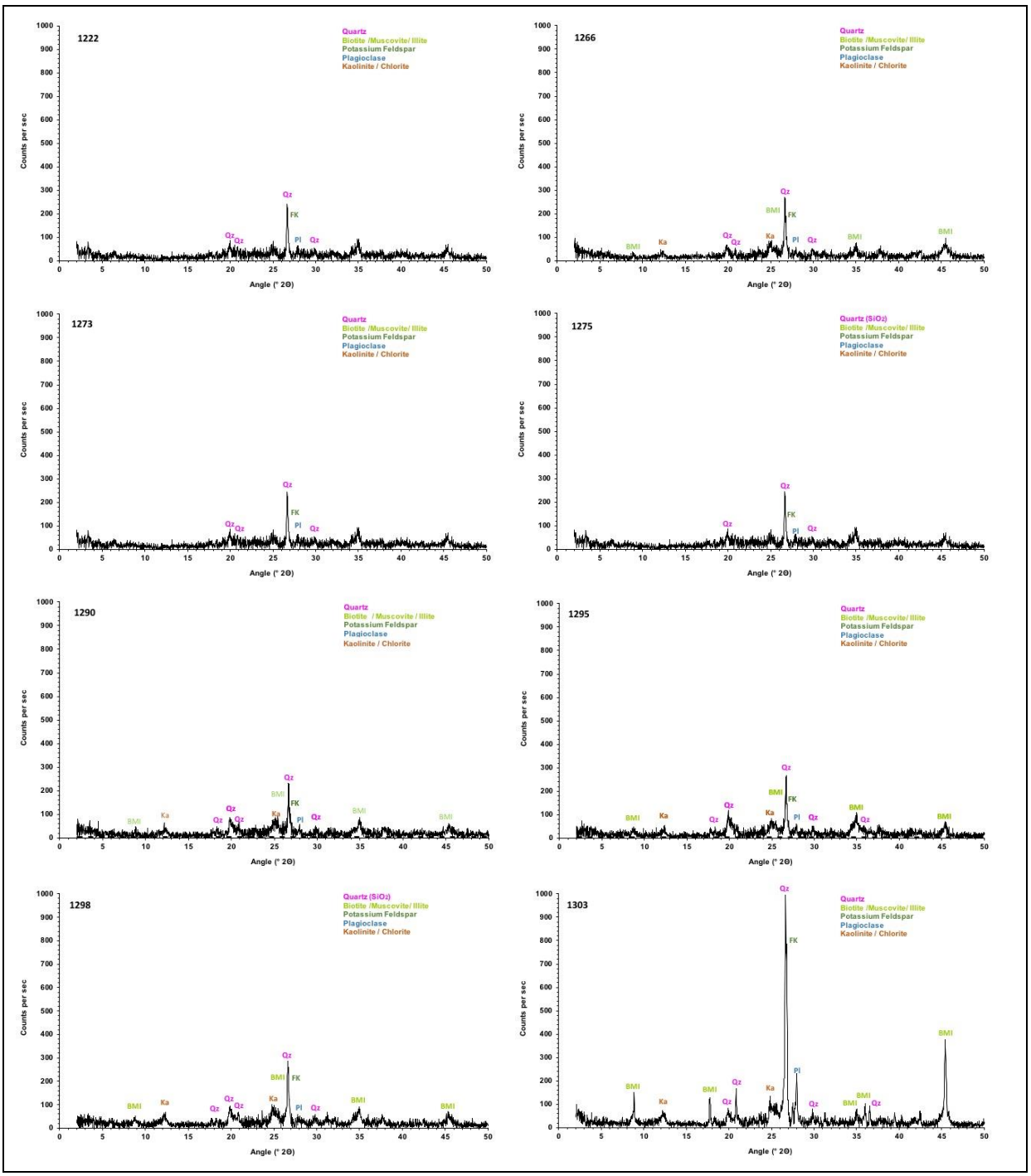

Figure 12. XRD of clay extraction for trench M5 samples. Note the order of the stratigraphy reads from the top left (1222) to bottom right graph (1303).

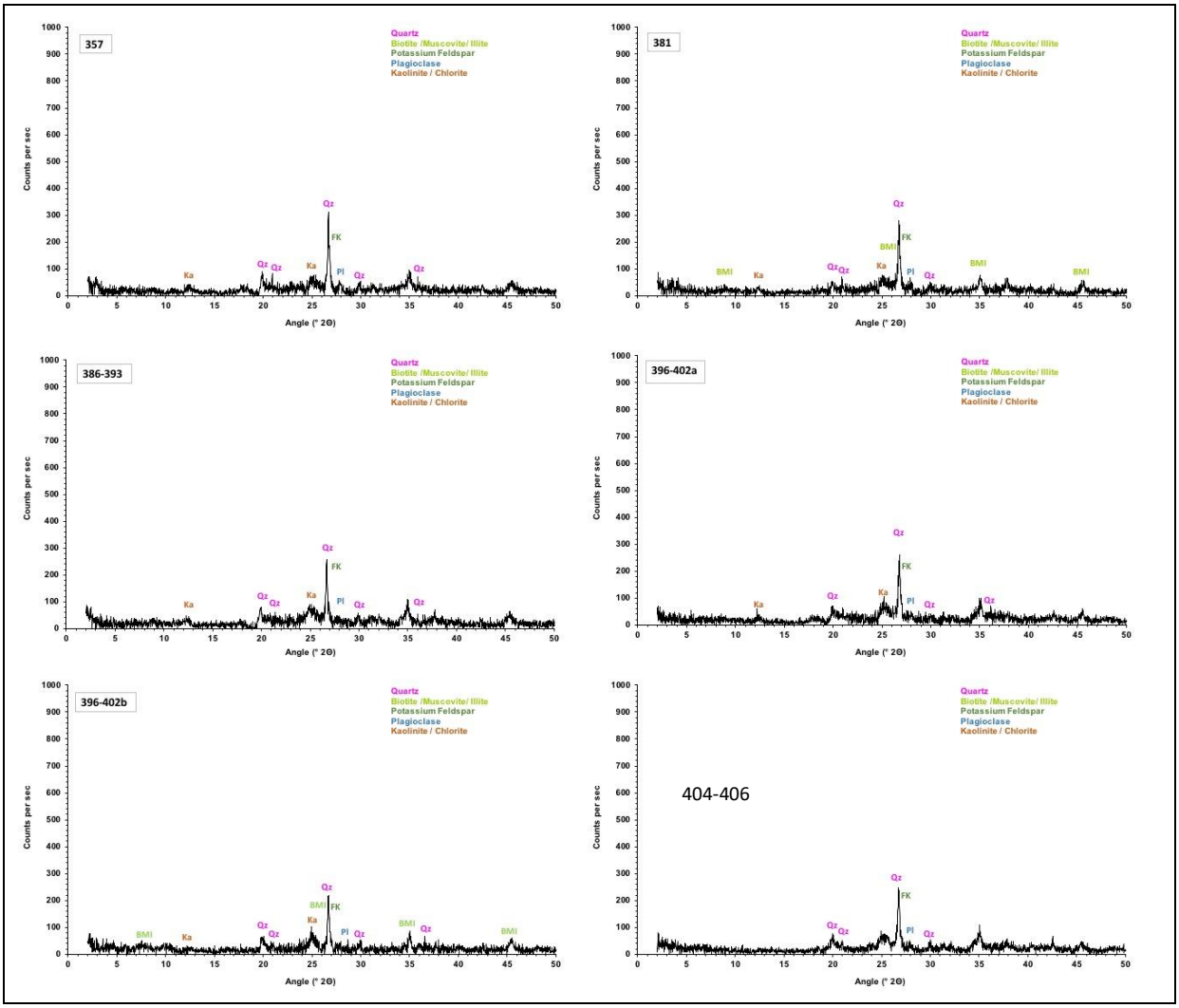

Figure 13. XRD of clay extraction for trench T1 samples. Note the order of the stratigraphy reads from the top left (357) to bottom right graph (404-406).

Subsequent XRD analysis to differentiate between their XRD patterns is being developed as each has unique water holding capacity in their interspaces and thus, a differential d-spacing upon de-hydration (Chipera & Bish, 2001). Despite the general low peak intensity and high degree of background noise of these samples, the presence of quartz is evident in every sample from all 3 trenches and prevails over the other minerals (Figures 12 & 13). The relative peak intensity of quartz can be attributed to its high degree of crystallinity and resistance to weathering resulting in relatively large size crystals, even in the clay-sized fraction.

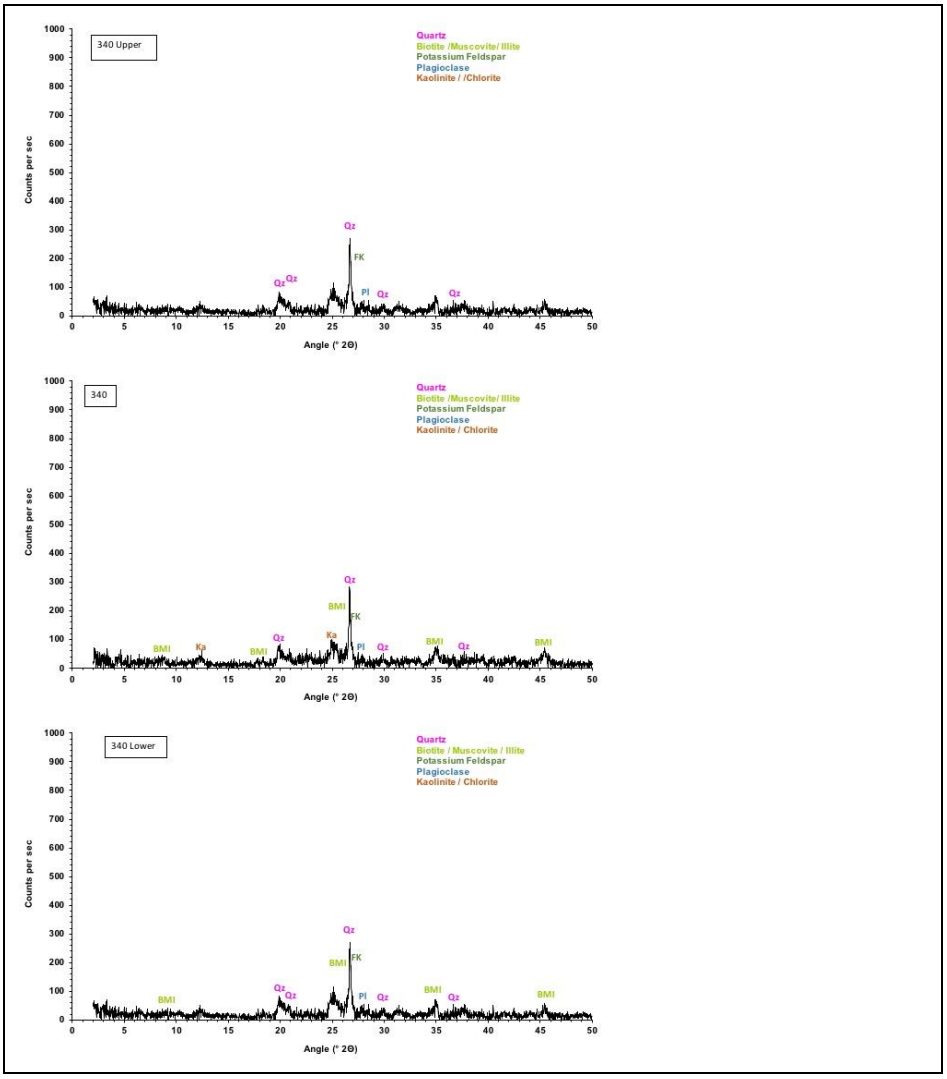

Figure 14. XRD of clay extraction for trench T1A samples 340 upper, 340 & 340 lower.

Hard quartz contained in a sample can often self-grind the other materials around it, particularly soft materials like clays, destroying their structure (Zhou et al, 2017). Reynolds and Bish (2002), demonstrate that just 10 minutes of grinding kaolinite resulted in fully disordered material that produced no peaks at all on XRD analysis. Our samples contain quartz prominently and so our preparation process was altered specifically to minimise any excessive breakdown of mineral structures within the clay extractions in order to optimise the results. The results can be interpreted as quartz self-grinding during glacial and fluvial processes (except 1303) and that the majority of the clay sized particles for each sample are nano-crystalline or highly disordered material.

It is reasonable to deduce that the clay sized fraction of the soil material in the foundation is made up of quartz, highly-disordered, nano-crystalline micas and inactive clays of varying chemical compositions with impurities. There are also traces of potassium feldspar (FK) and plagioclase (Pl). The speciation of clays in a soil can define the mechanical behaviour of the material as the differential interlayer energy dictates their resistance to plastic deformation. The clay sized particles in all of the foundation samples contain inert quartz, micas and inactive clays - illite and kaolinite. These clays have greater interlayer energy (Berthonneau et al., 2017) and as such will exhibit non-plastic behaviour. (Andrade et al., 2011) During an earthquake this would result in the flexibility of

the foundation materials allowing them to sway with ground movements without structural failures. Furthermore, the inert nature and low hydrological capacity of these materials would not restrict the drainage of water out of the foundation profile, making them less susceptible to liquefaction, is a major cause of earthquake damage.

3.3 Micromorphology and complementary XRF analyses

Table 6. Summary of Trench M5 and T1A Thin Section Descriptions

	Coarse Mineral Matter (>63um)							Fine Mineral Matter (<63um)					Organic Material					Pedofeatures				
Slide	Quartz	Fine Quartz	Mica	Ceramic	Fine Sandstone	Siltstone	Feldspar	Relative Distribution	Matrix	Silty-Clay Nodule	Silty-Clay Nodule (black amorphous inclusion)	Diatom Inclusion	Black Amorphous	Yellow Amorphous	Charcoal	Fungal Spore	Calcitic (shell)	Textural Clay Infill	Silty Clay Cap	Layered Clay	Crypto-crystalline Iron	Crypto-crystalline Root
M5 1222	**		*	*	***			Enaulic			*						*					
M5 1266	**	**		*				Gefuric	**				*	*	*			*				
M5 1273	****	**	**	**				Gefuric			**		*		*							
M5 1275	****		**	**		*		Gefuric	**		**		*	*	*			*			*	
M5 1290	***		**				*	Gefuric	***		*											*
M5 1295 Upper	••		•					Gefuric	••••		•											
M5 1295 Lower	**		**		*			Gefuric	***		*							*			*	
M5 1298	***		**	**	*			Gefuric		*	*					*			*	*		
M5 1303	*		*					Porphyritic	****			*	*					**			*	
T1A 339	**	**	**					Porphyritic	**	**	*							*			*	
T1A 340	**		*					Porphyritic	****				**	*				***			*	

Frequencies following Stoops et al., (2003)

*****	>50%	Dominant
****	50-30%	Common
***	30-15%	Frequent
**	<15-5%	Few
*	<5%	Very few

Abundancies following Stoops et al., (2003)

*****	>20%	Very abundant
****	10-20%	Abundant
***	5-10%	Many
**	2-5%	Occasional
*	<2%	Rare

3.3.1 Trench M5

Starting at the base of Trench M5, and the underlying environmental soils 1303 is dominated by silt sized particles comprised largely of linear mica sheets (Figure 15). These are finer at the base of the section increasing in size higher in the section with a coarser mica band at the top. These are preferentially orientated horizontally. Coarse sand mineral grains are limited in occurrence but with one quartz grain that is, unusually, significantly weathered (frost shattered). The fine material b-fabric between the mica sheets and quartz grains is linear and speckled and the related distribution is porphyritic. There is a small amount of organic matter and rare occurrence of diatom inclusions.

M5 1303

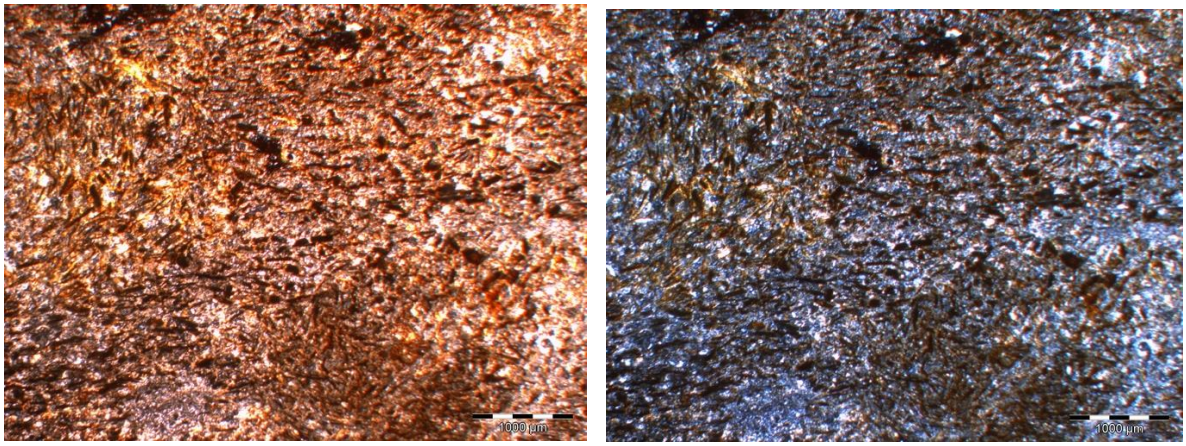

PPL **XPL**

Figure 15. Thin Section photographs of 1303 displaying orientated micas

There are rare pedofeatures of cryptocrystalline iron and occasional textural clay infills. This thin section is characteristic of a fluvial setting. The orientated grains and the microstratigraphy indicate a river system running through a catchment containing schist and carrying small amounts of organic debris. The linear b-fabric suggests the presence of clays that orientate under pressure. The iron pedofeatures suggest that this environment was periodical wet and dry allowing for redox reactions to occur in cycle. From the undisturbed nature of the aligned mica grains it is evident that this context is a natural environmental setting underlying the temple foundations.

M5 1298

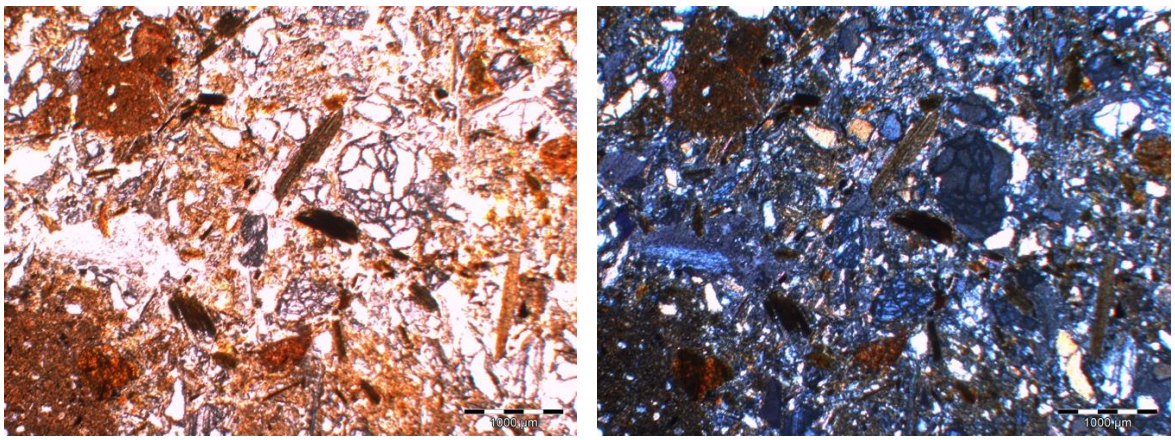

PPL **XPL**

Figure 16. Thin Section photographs of 1298 displaying weathered quartz grains.

Context 1298 is fundamentally different to the underlying 1303. Here minerals not present in the underlying environmental setting are evident and much coarser particles, with a distinct decrease in the frequency of fine mica grains. There is a lack of organisation or orientation of coarse grains, a speckled fine mineral b-fabric and with a gefuric related distribution. There are occurrences of sandstone fragments and highly weathered quartz grains (Figure 16). There are two types of silty clay nodules, one has fine organic black amorphous material embedded within it and the other is pure silt and clay that is not apparent in any of the other contexts.

M5 1298

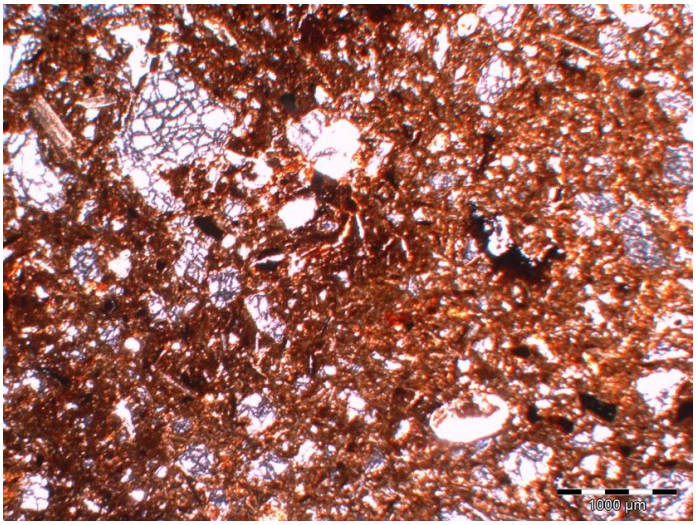

PPL

Figure 17. Thin Section photograph of 1298 displaying ceramic with coarse quartz embedded.

Ceramic additions with embedded coarse quartz grains are also evident (Figure 17). There are layered clay and clay cap pedofeatures. The random organisation of the coarse material shows a change from the underlying fluvial environmental setting and suggests that the material has been disturbed and mixed. This is in keeping with the theory that this material was moved from its original location to be deposited here as a component of the lower mandala of the temple foundations. The appearance of ceramics also indicates cultural additions. In similar archaeological settings clay nodules such as the ones seen here are analogous of mud brick wall fragments. The pedofeatures and the extent of the quartz weathering suggest a freeze thaw action and exposure at the surface for some time – most likely prior to deposition. The presence of metamorphosed sandstone fragments indicates contrasting sediment sources.

M5 1295 UPPER

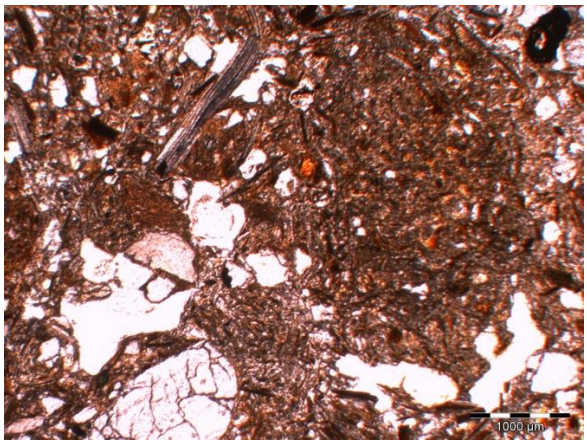

PPL

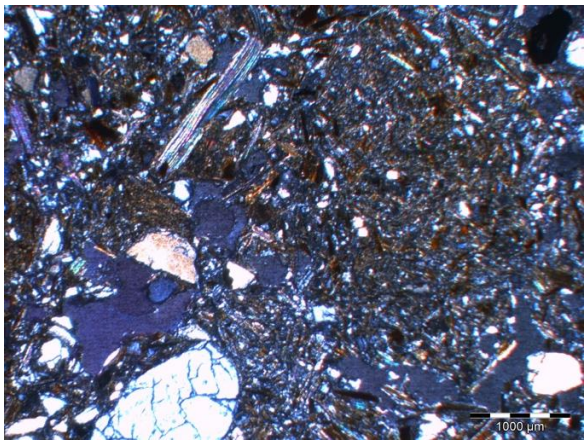

XPL

M5 1295 LOWER

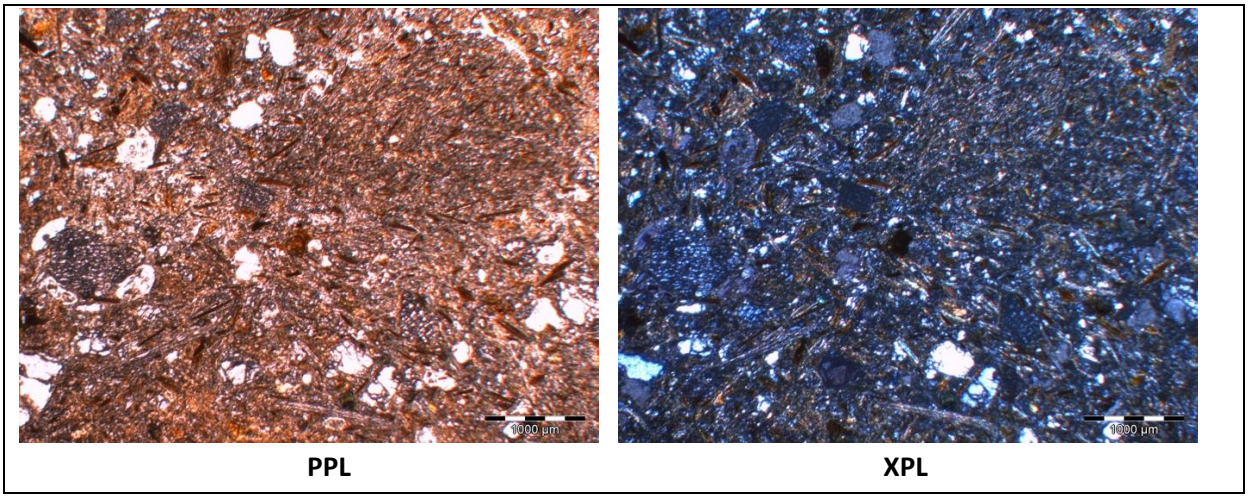

Figure 18. Thin Section photographs of 1295 showing upper and lower micro-horizons.

In 1295 there is much less quartz, with individual grains weathered from the fine metamorphosed sandstone fragments but which are themselves much less weathered than in 1298. There is a sharp boundary between the upper and lower areas with alternating fine and coarse dominated micro-horizons. There are more coarse mica grains in the lower section, the upper section is mostly fine mica (Figure 18). Fine sandstone, textural clay infill and cryptocrystalline iron pedofeatures are present only in the lower micro-horizon. Silty clay nodules with black amorphous inclusions are present only in the upper section; there are no ceramic additions. Silty clay nodules are of two types, one light coloured and one dark coloured (Figure 18a). XRF analyses indicates the contrasting elemental composition of these nodules with the light clay having a greater silica and iron concentration; there are also contrasts observable in trace element composition indicating a contrasting source for the clay nodules. The enhanced levels of soil amendment indicators, phosphorus (P) and magnesium (Mg), suggests that the dark clay nodules originated from an agricultural soil (Figure 18b). The fine mineral material b-fabric is speckled; related distributions are gefuric. These characteristics are in contrast to the material in the stratigraphy below and suggest contrasting origins for the materials. These contrasts include a lesser extent of quartz weathering and iron pedofeatures that reappear in the lower section after being absent from the horizon below 1298.

Figure 18a: Silty clay nodules in the M5 sequence, observed in the field; note light and dark colours

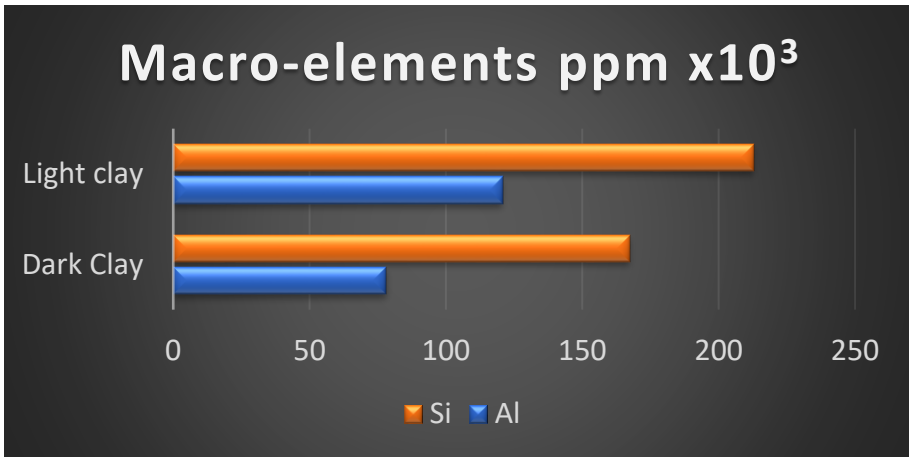

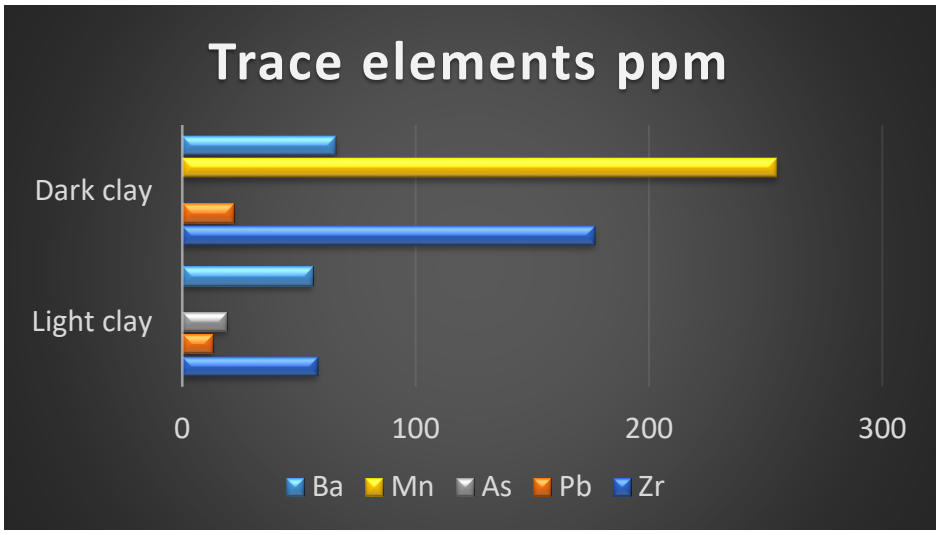

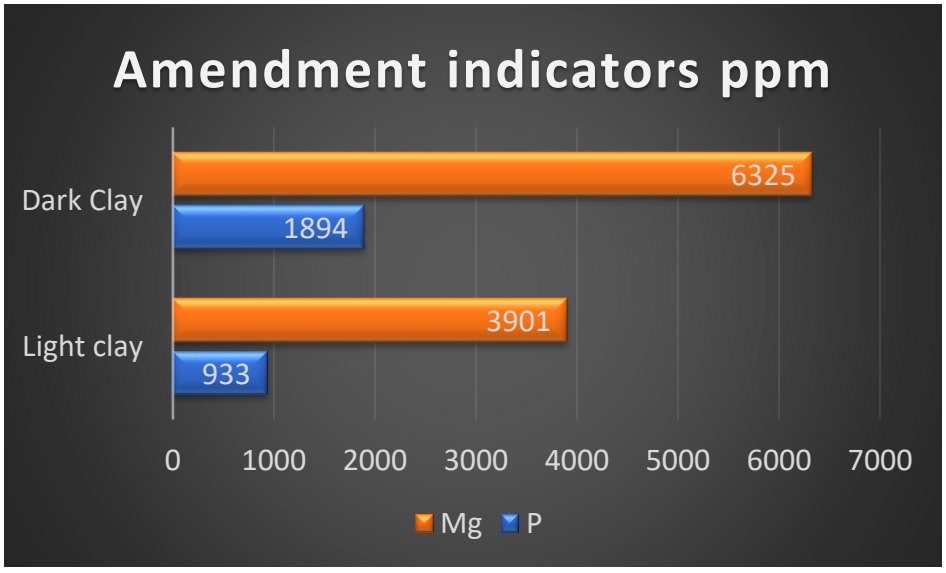

Figure 18b. XRF analyses of clay nodules, demonstrating contrasting origins of dark and light nodules. Values presented are the average of three field readings.

M5 1290

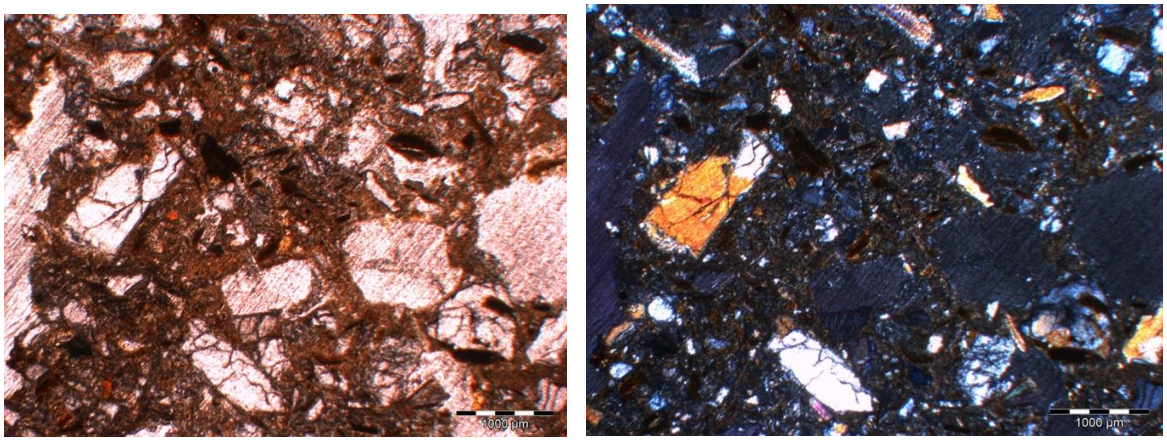

PPL **XPL**

Figure 19. Thin Section photographs of 1290 showing variable, coarse grains.

In 1290 there is frequent quartz, few mica, very few silty clay nodules and the first occurrence of feldspar; coarse grains are not orientated. There is a degree of organisation, but it is to a far lesser extent than the context below; this material is less sorted and coarser in general, and the grains are more variable (Figure 19). The related distribution continues as gefuric with the b-fabric speckled. Pore spaces are larger. The new occurrence of feldspar suggests that this is again different material drawn from a contrasting location. The lack of orientation of the mica grains indicates that this material was disturbed and mixed and supports the idea that the material was extracted and moved from some distance to the site location. The coarse organic material could indicate the cultural addition of ritual offerings as detailed in the Sanskrit text Mãnasarã.

M5 1275

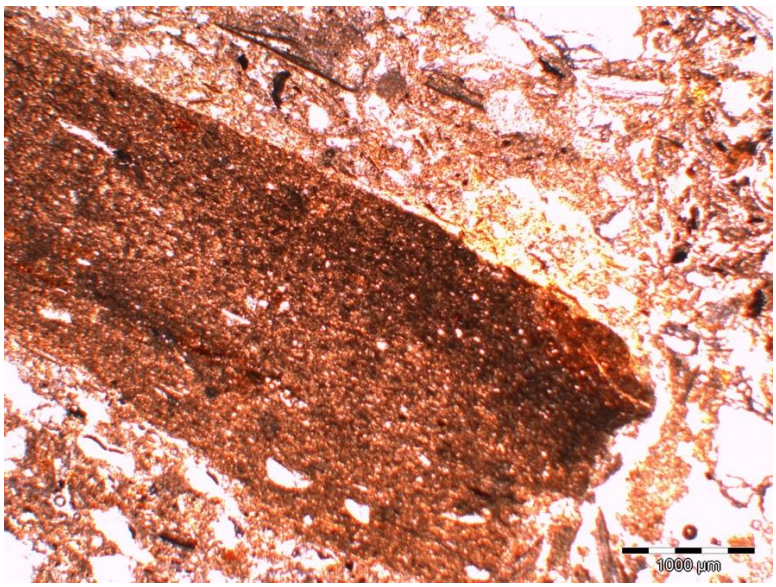

PPL

Figure 20. Thin Section photograph of 1275 showing burnt, fine grained ceramic.

1275 is predominantly quartz with some mica and a fine metamorphosed siltstone fragment. The related distribution is gefuric with the b-fabric being speckled. There are also ceramics present, some

of which are burnt (Figure 20). Silty clay nodules are smaller and red/brown in colour not seen in any other context but these still contain the organic black amorphous material. There is frequent organic black amorphous material (not in inclusion), yellow amorphous material and large charcoal fragments throughout, not previously seen before in the lower (or upper) contexts. Field XRF analyses of this context have given particular attention to phosphorus (P) concentrations (ppm) with this element a proxy evaluation of organic amendments of the sediments given it ubiquity in organic materials and its retention on soils and sediments after organic decomposition. Figure 20a demonstrates enhanced P values in context 1275 (and in context 1273 above) relative to other contexts in this profile, confirming the enhanced organic content observed in thin section. Similar pedofeatures – clay infill and cryptocrystalline iron – to previous contexts are visible with the difference that the clay is yellow in colour.

It is likely that the siltstone is a fine clay-based ceramic and the blackened edge is due to burning. This material is typical of high quality ceramic pots used in rituals and is significantly different to the fine-sandstone ceramic material with coarse quartz seen in previous contexts. This theory is supported by the abundance of black and yellow organic material, large charcoal fragments, which could point to a ritualistic burning on this context at the time of its deposition or of additional cultural organic components to this context as part of a ritual offering as reflected in the enhanced P concentrations. It is interesting to note that this is the first layer of soil in the upper mandala.

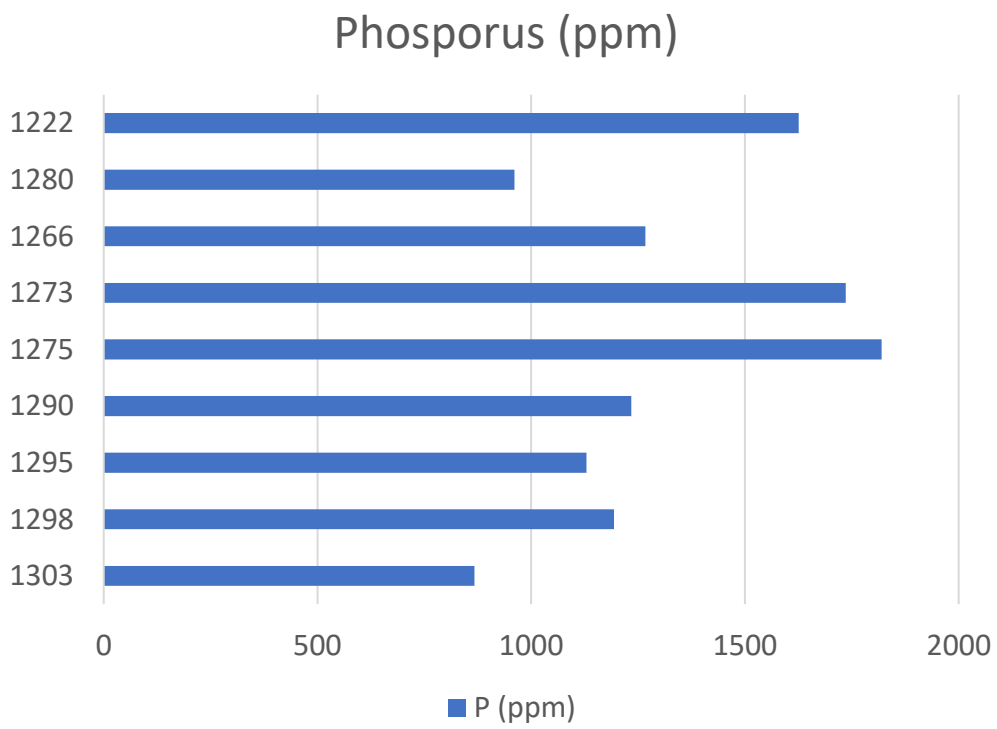

Figure 20a: Field XRF phosphorus concentrations in Trench M5 contexts.

M5 1273

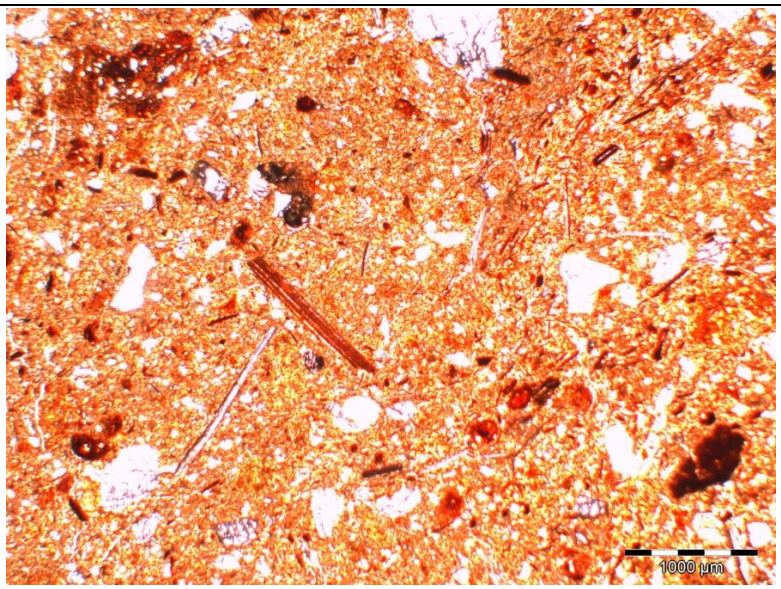

PPL

Figure 21. Thin Section photograph of 1273 showing a coarse grained ceramic fragment.

In 1273 we see the presence of fine grained quartz for the first time in the stratigraphy. The mineral material is coarser than previously and a lack of fine grained matrix material. There is an abundance of quartz and mica is present. The related distribution is gefuric with the b-fabric being speckled. There is a metamorphic grain that could not be identified but has not been observed in the lower stratigraphy. We see the re-emergence of ceramics containing coarse grains of quartz. Similar to the previous context, there is the occurrence of silty clay nodules with organic inclusions together with a small amount of black amorphous material and charcoal fragments throughout. This again is very different material to any of the previous contexts. The abundance of quartz is similar to 1275 below but there is fine quartz for the first time. The presence of ceramics is again similar to 1275 but these are fundamentally different to the fine-grained ceramics of 1275 and much more comparable to those seen in the lower mandala at 1298 (Figure 21). The lack of fine grained material is distinct from the other contexts with the exception of 1298. The silty clay nodules return to a colour as seen in all of the previous contexts except 1275.

M5 1266

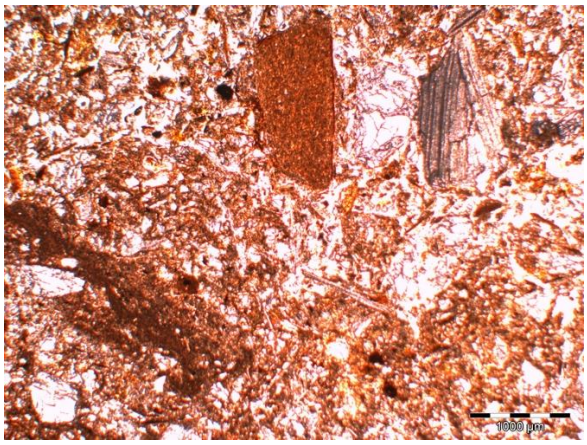

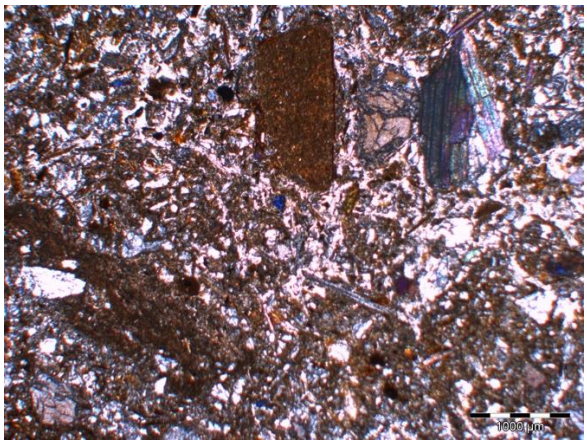

PPL **XPL**

Figure 22. Thin Section photographs of 1266 displaying the brown coloured fine grain material.

In 1266 we see a continuation of the fine quartz material, but with mica absent for the first time in the stratigraphy. The fine material is brown in colour, different to the rest of the contexts (Figure 22). The pore spaces in this thin section are distinctly larger than previously seen and just one small fragment of ceramic is present. Organic material is present in the form of black and yellow amorphous material and charcoal fragments, and there is textural clay infill pedofeatures. The pore space indicates biological activity and explains the disturbed, mixed nature of the soil with no real organisation or structure. The lack of mica, compared to the other contexts where mica has been consistently present, suggests that this is again a new, distinct material and the brown fine-grained material is suggestive of high organic content such as is found in a topsoil material.

M5 1222

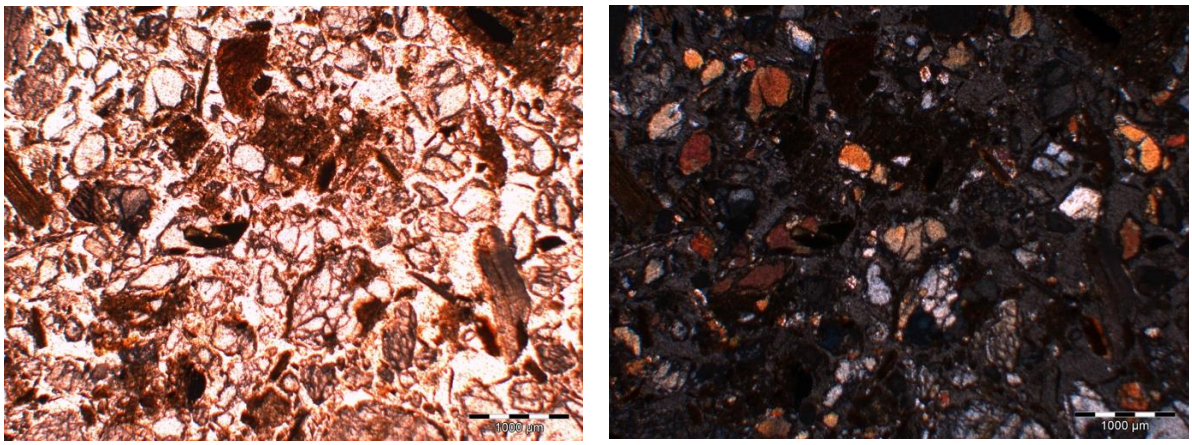

PPL **XPL**

Figure 23. Thin Section photographs of 1222 showing a lack of fine grained material.

The material in 1222 is characterised by a relative lack of fine material with only a small proportion of the section evident as silty clay nodules with organic black amorphous material (Figure 23). A high proportion of coarser material is dominated by fine sandstone fragments in greater frequency than previously seen in the lower contexts 1298 and 1295. The related distribution between the coarse quartz and micas, and the fine material is enaulic, distinctly different from the rest of the stratigraphy. Interestingly, within one of these there is a calcitic fragment of what looks like shell. Some of the mica grains here are contorted from metamorphosis. The environment that the clay nodule containing the shell could potentially have come from is unlikely to have been from within the Kathmandu Valley. The metamorphic nature of the micas has not been observed in the other contexts and so this indicates that this upper context is again from a different environmental location to the other materials within this stratigraphy.

Thin section analysis of the environmental samples, 340 and 339 from trench T1A, confirmed that their micromorphology does not match any of the contexts within the foundation profile. Sample 340 is organised in a distinctive way and is most similar to the upper section of 1303 in that they are both porphyric, have few quartz grains, very few mica and fine grain material is dominant. Organic amorphous material and cryptocrystalline iron occur at low frequencies in both and textural clay infills are more frequent (Figure 24). This material is characteristic of a low energy alluvial setting that periodically dried out.

T1A 340

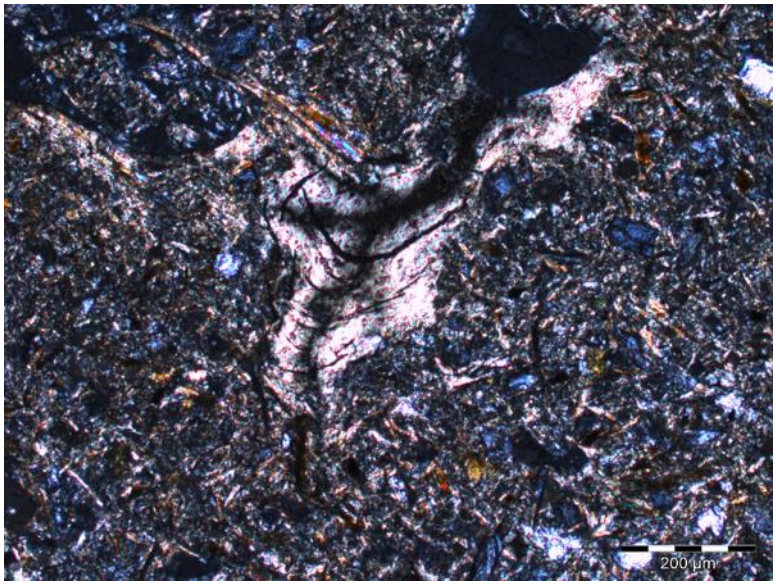

XPL

Figure 24. Thin Section photograph of 340 displaying an excellent example of a textural clay infill.

Sample 339 is also unlike any one of the contexts as it is porphyric, contains both coarse and fine, quartz and mica that is not seen in any of the foundation contexts (Figure 25). This agrees with the dual-peaked shape of the PSD and the roundness of the grains indicates a higher energy river setting. Furthermore, this sample has discrete silty-clay nodules with quartz embedded within that is distinct from any of the other silty-clay nodules seen throughout the foundation profile. This strengthens the premise that the foundations materials were not taken directly from the land adjacent to the temple location.

T1A 339

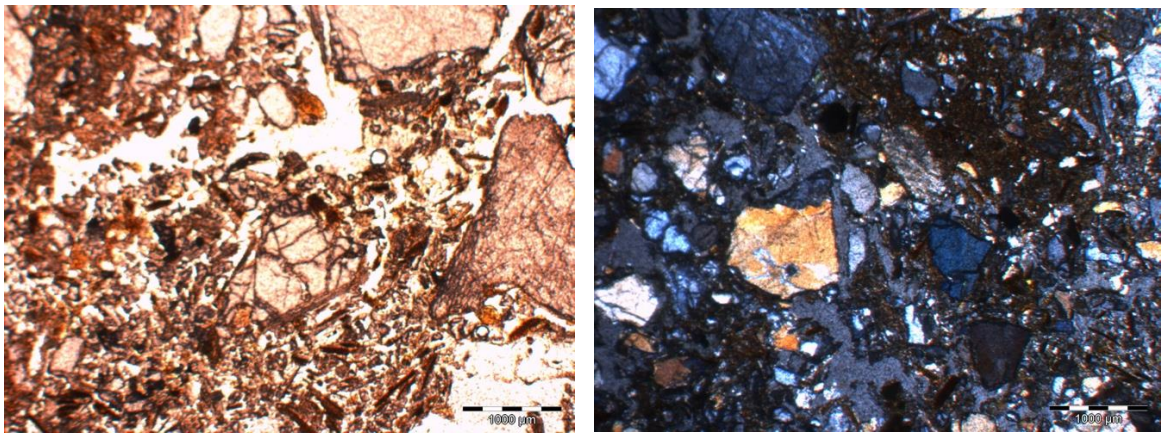

PPL **XPL**

Figure 25. Thin Section photographs of 339 showing both fine and coarse grains of quartz and mica.

These micromorphological analyses add details to our knowledge of the nature of the foundation materials and confirms that each context is unique as demonstrated in the PSD analysis. Furthermore, the identification of minerals quartz, mica and some feldspars in these thin sections consolidates the results from the clay analysis by XRD.

4: Discussion

4.1 What is the nature of the infill sediments?

Pairwise comparisons of PSDs indicate that the uppermost contexts in trench T1 and M5 are individually similar to each other and share a common down profile pattern, with the one exception of sample 1266 in trench M5 not having an equivalent in trench T1. The surface of sample 1290 from trench M5 corresponds to the beginning of a walled compartment of a lower (and inner) mandala within the foundation design. This section contains different material based on the PSDs and mineral composition of equivalent depths within trench T1. In trench T1 there is no lower mandala evident and each layer of soil is thicker in depth. This indicates that across the foundation the layering sequence is likely uniform in an upper mandala. Where there are lower mandala compartments, these results suggest that there is likely to be further layers containing more unique and distinct soil materials.

The analysis of the thin sections revealed the highly weathered state of some of the quartz and mica grains. In sample 1266 and 1273 it is noted that there are finer quartz and mica grains. This could offer an explanation as to why the X-ray diffraction analysis for the clay size extract had such high levels of background noise. It is likely that a proportion of the clay sized particles are highly weathered, nanocrystalline mica and quartz grains.

The uniqueness of the PSD and microstructure of each context combined with the lack of down profile sorting suggests a laying down of materials in a defined order that is not naturally occurring. The lack of orientation of the mica grains noted in the micromorphological analysis indicates a likely mixing and moving of these materials prior to deposition.

The PSD results and micromorphological analysis of the different samples within the foundations revealed that this infill material does not match the environmental material in the local vicinity. Characteristically, soil sediments in the Kathmandu Valley are clay rich (Maskey, 2013) but all of these contexts contain low percentages of clay sized particles. Furthermore, the variety and uniqueness of each context suggests a careful and specific selection of materials from different sources with environmentally distinct settings.

4.2 Is there evidence of the ritual practice detailed in the textual sources?

The differential layering in the upper and lower mandalas of the foundation link to the ritual detailed in Sanskrit texts and is the first suggestion that this was an integral part of the foundation construction process at Kasthamandap. The *Brhatsamhitã, Mãnasarã* and *Mayamata* require that each mandala compartment in the foundation be dedicated to a specific deity and the offerings and blessings should be individually tailored to each compartment in order to please the gods. The *Mãnasarã* explicitly states the exact minerals and herbs to be included in each plot, while the *Brhatsamhitã,* requires that this process must begin in the North East corner of the foundation but the *Mayamata* indicates that the offerings should begin with those to Brahma in the centre and continue to the East and then in a clockwise direction through the different compartments and deities.

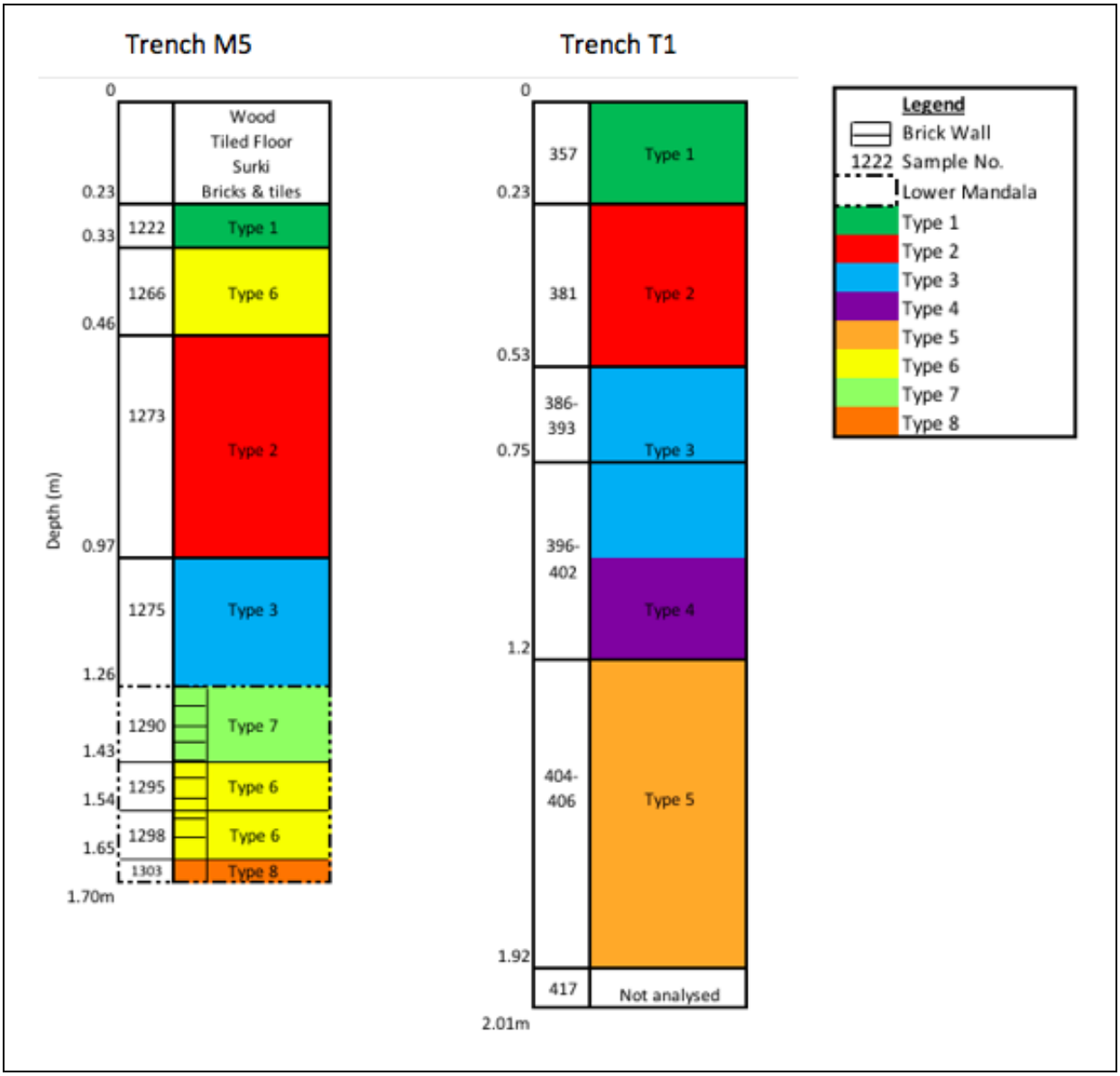

Figure 26. Interpretive stratigraphic profile of the foundation infills to highlight down profile relationships between trench M5 and T1.

The unique contexts in down profile sequence of the foundation infill materials combined with the sedimentary layering arrangement of these clearly indicates a careful and deliberate cultural process. Furthermore, the cultural inclusion of high quality ceramics at the interlayer between the upper and lower mandala, signal an important event as these are typically reserved for religious rituals and offerings to the gods. There is also a significant proportion of ceramics, although of a lesser quality, in the uppermost layer of soil infill. All three of the texts mention auspicious pots filled with water being arranged on the foundation after the infill has been added. It is the last stage before the construction can continue with the erection of the superstructure. The *Brhatsamhitã* is the vaguest and mentions only pots of water, flowers strewn and the reciting of chants to worship the centre deity with scents, incense, cloth, food, gold and liquor. While the *Mayamata* details the careful placing of these ceramic pots in an arrangement across the surface of the newly laid foundation as architects and builders gather to pray to Brahma. It describes how 25 pots are filled

with water, covered with linens and flowers while a ritual chant is recited as the foundation is 'installed' with water to bless the foundations. Interestingly, the *Mãnasarã* describes this process almost exactly to the *Mayamata* except that this ritual is repeated in full twice with a 'sacrifice to the fire' of plants, ghee, seeds and rice between the two.

The individuality of every context and the clear dissimilarity to the material in the local vicinity shows a careful and specific selection of materials. Both *Mãnasãra* and *Mayamata* specify that seven types of earth are to be deposited within the 4 walls of the foundation and go on to dictate the locations that these materials must be sourced. They both agree on from a river, a mountain, an ant-hill, a crab-hole and from a cowshed or the horn of a bull; tusk of an elephant; ploughshare. But then they disagree on the final two locations; a field and a pond, or a seashore and the top of trees.

All these factors in combination suggest that it is highly likely that the ritual detailed in the Sanskrit texts was employed in the construction process of Kasthamandap.

4.3 Did the foundations contribute to the earthquake resilience?

Soil-structure relationships are highly complex and the nonlinear nature of the behaviour of soils under varying intensities and different types of seismic pressure makes it very difficult to infer the exact physical response of these materials to the earthquake (Gautam, 2017). Furthermore, there are no studies on the dynamic behaviour of the sediments in the Kathmandu valley to determine if the foundation soils beneath Kasthamandap locally amplify or de-amplify the seismic waves. De-amplification correlates to soil nonlinearity thus this must be accounted for in order to accurately predict soil behaviour (Chamlagain & Gautam, 2015). However, from the lack of damage to the foundations post-earthquake it is clear that this ancient method of construction with introduced soil is an effective contributor to earthquake resilience (Coningham et al., 2016). All the samples have low clay percentages in the less than 2mm fraction and a greater proportion of coarser silts and sands. These materials are all preferential in earthquake resilient design of foundations as they provide adequate ductility of the foundation structure and allow water to drain away, out of the profile faster (Gautam, 2017). This restricts pooling of water under the structure that causes the material to be less susceptible to liquefaction in the event of an earthquake (Gautam et al., 2017).

Current X-ray diffraction data indicates that that the clay sized fraction contains no (or very limited occurrence) of actively shrinking and swelling clays. Due to their swelling behaviour under wetting (due to water molecules filling their interlayer space) and subsequent contraction on drying, (Berthonneau et al., 2017) active clays can seriously undermine the stability and structural integrity of any building. These types of clays cause larger voids and poor binding in the masonry of foundations. During an earthquake their presence can cause the delamination of bricks causing the walls of the foundation to move independently from each other and creating structural damage (Gautam et al., 2016a). Furthermore, these clays retain water and would restrict drainage causing a greater risk of liquefaction. The absence of these minerals despite the wide variety of materials within the foundation infill suggests that there may have been careful selection, sorting, organisation and arrangement of these materials has a specific purpose to mitigate earthquake damage. The hydrologically inactive clays, Kaolinite and Illite that are present in these materials,

have low shrink – swell capacity and retain limited or no water within their chemical structures and as such, do not restrict the free draining of water out of the profile**.** The coarse particles contribute to the minimisation of water in the foundation profile and hence ensure the stability of the superstructure above as saturated material is more susceptible to liquefaction (Gautam et al., 2017). This again points to the foundation construction ritual being based on a cultural knowledge of how to design foundations in order to help structures to resist earthquake damage. The lack of hydrologically active clays in the foundations materials could have arisen either by preferential selection of soils or by sorting the material to exclude these particles.

5: Conclusions

This paper has assessed the nature of foundation fills at Kasthamandap, Kathmandu Valley. The sediments are culturally arranged and evidence a ritual construction process that historically was common practice in South Asia. The components of the foundation and the method of their construction apply core principles of earthquake resistant strategies and contribute to the resilience of the superstructure of Kasthamandap. This traditional method of foundation design highlights a cultural knowledge of earthquake damage mitigation transmitted in the form of ritual texts.

This work offers a new narrative of the construction and history of Kasthamandap and allows an insight into a time in Kathmandu's history that is sparsely documented. Furthermore, this project contributes new details about temple foundations that have not previously been scientifically recorded. This information is multifaceted, supplies details of the construction not previously understood and will add to the UNESCO World Heritage Status of Kasthamandap despite the superstructure collapse. The paper builds a knowledge about early temples in the Kathmandu Valley that will aid in the conservation of heritage in this region that continues to be at risk following the 2015 Gorkha earthquake.

These new lessons about ancient temple design, intangible heritage and earthquake resilience can be applied to new thinking on the efforts reconstruction of Kasthamandap as not only are the original foundations materials seismically robust they add resilience to the superstructure. This knowledge could help to inform civil engineers on the best materials and methods to use in the rebuilding in a way that retains the maximum authenticity and ensures the safety of the new building into the future. Furthermore, these results can be modified or broadly applied further afield to heritage in disaster prone regions.

There is more work to do to better understand the soil materials used in temple foundations. The source of foundation materials could be investigated to further explore the ritual aspects of the foundation construction. This could be achieved by sediment fingerprinting in order to characterise location or environmental settings from which the soils originated before being moved and deposited in the foundations. It would also be of interest to investigate the organic components contained in the compartments of the mandalas to determine if they relate to the sequence of offerings outlined in the textual sources. Chemotaxonomy could be applied with the use of leaf-wax as biomarkers to further assess the prominence of the Sanskrit texts in detailing construction

processes in Kasthamandap or the Kathmandu Valley in the seventh century, as has been undertaken at Lumbini.

Furthermore, the highly variable response of the ground behaviour to earthquakes in the Kathmandu Valley reflects the geologically diverse sub-surface sediments within a small spatial area (Gautam, 2017). An investigation into the sediments below the foundations could shed light on the ground motion behaviour that occurs locally underneath Kasthamandap. This type of study has not been conducted in any great detail for any localised parts of Kathmandu despite the fact that it could shed light on the vulnerability of structures and how this might be mitigated by traditional foundation constructions.

This paper demonstrates that geoarchaeological methods can be utilised effectively to bring new insight and understanding to the nature of foundation construction and earthquake resilience design. The new narratives have been created detail Kasthamandaps' history, foundation construction and the possible link to a historical, cultural knowledge of earthquake resilience techniques in Nepal. These lessons can be brought to new aspects of South Asian heritage conservation and, can be applied to future projects such as reconstructions of the other World Heritage properties in the Kathmandu Valley also damaged in the 2015 Gorkha Earthquake.

Appendix 1: Field soil strength (penetrometer)

Context	Bulk Density (g/cm^3)	Mean Resistance (and range) Kg/cm^2
1222	0.76	0.25 (0.25-0.25)
1280	0.79	2.67 (2.57-2.50
1266	0.86	2.67 (2.57-2.50)
1273	0.88	3.08 (3.50-2.75)
1275	1.05	2.67 (3.25-1.75)
1290	1.01	3.08 (3.50-2.27)
1295	0.99	0.58 (0.75-0.50)
1298	0.99	0.58 (0.75-0.50)
1303	0.88	3.00 (3.25-2.75)

Trench M5 (HMD): Field soil strength indicators of fills

Trench 1 Context	Field texture class	Bulk Density (g/cm^3)	Mean Resistance (and range) Kg/cm^2
357	mszl	0.76	1.05 (1.50-0.50)
381	mszl	0.81	3.08 (4.25-1.50)
386-393	msl	0.84	2.50 (3.50-1.75)
396-402a	mls	0.79	2.52 (2.75-2.00)
396-402b	mls	0.79	1.92 (2.50-1.25)
404-406	ls	0.86	2.08 (2.75-1.75)
T1a. 346	mls	0.86	2.50 (3.50-1.75)

Trench 1 (HMD): Field soil strength indicators of fills

References

Acharya, P. (1994). Architecture of Mãnasarã. Volume 4. New Delhi: Oriental Books Reprint Corporation.

Andrade, F., Al-Qureshi, H. & Hotza, D. (2011) Measuring the plasticity of clays: A review. *Applied Clay Science*, 51, pp.1-7.

Berthonneau, J., Hoover, C., Grauby, O., Baronnet, A, Pellenq, R. & Ulm, F. (2017) Crystal-chemistry control of the mechanical properties of 2:1 clay minerals. *Applied Clay Science*, 143, pp. 387-389.

Chamlagain, D. & Gautam, D. (2015) Assessment of Urban Seismic Hazard due to 2015 Gorkha Seismic Sequence. 14th International Symposium on New Technologies for Urban Safety of Mega Cities in Asia. 29 October.

Chipera, S. & Bish, D. (2011) Baseline studies of the clay mineral society source clays: Powder x-ray diffraction analyses. *Clays and Clay Minerals*, 49:5, pp. 398-409.

Coningham, R., Acharya, K., Davis, C., Kunwar, R., Simpson, I., Schmidt, A. and Tremblay, J. (2016). Preliminary results of post-disaster archaeological investigations at the Kasthamandap and within Hanuman Dhoka, Kathmandu Valley UNESCO world heritage property (Nepal). *Ancient Nepal*, 191-192, pp. 28-51.

Dagens, B. (1997). Mayamata: Treatise of Housing, Architecture and Iconography. Volume 1. Delhi: Motilal Banarsidass.

Dixit, A., Parajuli, Y. and Guragain, R. (2004). Indigenous Skills and Practices of Earthquake resistant construction in Nepal. 13th World Conference on Earthquake Engineering. Vancouver, 1 – 6 August 2004.

Gautam, D. (2017) Unearthed lessons of 25 April 2015 Gorkha earthquake (Mw 7.8): geotechnical earthquake engineering perspectives. *Geomatics, Natural Hazards and Risk*. Available: https://www.tandfonline.com/doi/full/10.1080/19475705.2017.1337653 [Accessed: 01 November 2017]

Gautam, D., Rodrigues, H., Bhetwal, K., Neupane, P., & Sanada, Y. (2016a) Common structural and construction deficiencies of Nepalese buildings. *Innovative Infrastructure Solutions*. 1:1

Gautam, D., Prajapati, J., Paterno, K., Bhetwal, K. & Neupane, P. (2016b) Disaster resilient vernacular housing technology in Nepal. *Geoenvironmental Disasters*. 3:1

Gautam, D., Santucci de Magistris, F., Fabbrocino, G. (2017) Soil liquefaction in Kathmandu valley due to 25 April 2015 Gorkha, Nepal Earthquake. *Soil Dynamics and Earthquake Engineering.* 97, pp. 37-47.

Jaquin, P. (2012) Influence of Arabic and Chinese Rammed Earth Techniques in the Himalayan Region. *Sustainability.* 4, pp.2650-2660.

Kinnaird, T. & Simpson, I. (2016) OSL dating of sediments revealed during rescue excavations at Hanuman Dhoka and Bhaktapur Durbar Square, Kathmandu, Nepal. *Scottish Universities Environmental Research Centre.*

Kunwar, R. (2017). Excavations: Post-disaster archaeological research in the Kathmandu Valley. Heritage at Risk: Pathways to the Protection and Rehabilitation of Cultural Heritage in South Asia. Kathmandu, 3 – 7 September 2017. Available: https://www.dur.ac.uk/cech/unescochair/workshops/heritageatrisk/

Langenbach, R. (2015) The earthquake resistant vernacular architecture in the Himalayas. In: M. Correia, P. Lourenço & H. Varum eds. *Seismic Retrofitting: Learning from Vernacular Architecture*. London: Taylor & Francis Group.

Maskey, P (2013) Disaster risk of cultural heritage sites of the Kathmandu Valley. Revisiting Kathmandu: Safeguarding Living Urban Heritage. International Symposium Kathmandu Valley, 25-29 November 2013. Available: http://unesdoc.unesco.org/images/0023/002317/231755E.pdf

Mirnig, N. (2017). Records in stone: ancient Kathmandu's inscriptions and texts. Heritage at Risk: Pathways to the Protection and Rehabilitation of Cultural Heritage in South Asia. Kathmandu, 3 – 7 September 2017. Available: https://www.dur.ac.uk/cech/unescochair/workshops/heritageatrisk/

Moore, D. & Reynolds, R. (1997) X-Ray Diffraction and the Identification and Analysis of Clay Minerals. Oxford: Oxford University Press. 378.

Niroumand, H., Zain, M. and Jamil, M. (2013). Various types of earth buildings. 2nd Cyprus International Conference on Educational Research. North Cyprus, 14 – 16 February 2013. *Procedia – Social and Behavioural Sciences*, 89, pp. 226-230

National Oceanic Atmospheric Administration (2017). National Geophysical Data Center, Significant Earthquake Database. Available: https://www.ngdc.noaa.gov/nndc/struts/form?t=101650&s=1&d=1 [Accessed: 01 November 2017]

Oldfield, H. A. (1860) The Market Place, Kathmandu' Available: http://www.asianart.com/articles/kasthamandap/index.html [Accessed: 01 November 2017]

Parkin, S. & Adderley, P. (2017). The Past Ubiquity and Environment of the Lost Earth Buildings of Scotland. *Human Ecology*, 45, pp. 569-583

Silveira, D., Varum, H., Costa, A., Martins, T., Pereira, H. & Almeida, J. (2012) Mechanical properties of adobe bricks in ancient constructions. *Construction and Building Materials*, 28, pp. 36-44

Simpson, I., Guttman, E., Cluett, J. & Shepherd, A. (2006) Characterizing Anthropic Sediments in North European Neolithic Settlements: An Assessment from Skara Brae, Orkney. *Geoarchaeology: An International Journal*, 21:3, pp. 221-235.

Simpson, I. (2017). Can we Rebuild Kasthamandap? New narratives of site formation processes through geoarchaeological investigation. Heritage at Risk: Pathways to the Protection and Rehabilitation of Cultural Heritage in South Asia. Kathmandu 3 – 7 September 2017. Available: https://www.dur.ac.uk/cech/unescochair/workshops/heritageatrisk/

Slusser, M. & Vajrãcãrya, G. (1974) Two Medieval Nepalese Buildings: An architectural and cultural study. *Artibus Asiae.* 36:3, pp.169-218

Stoops, G. (2003). Guidelines for Analysis and Description of Soil and Regolith Thin Sections. 1st Edition. *Soil Science Society of America*. Madison

Tiwari, S. (2017). Post-disaster archaeology: Heritage of Foundations of Temples of the Kathmandu Valley. Heritage at Risk: Pathways to the Protection and Rehabilitation of Cultural Heritage in South Asia. Kathmandu, 3 – 7 September 2017. Available: https://www.dur.ac.uk/cech/unescochair/workshops/heritageatrisk/

UNESCO (2017). Available: http://whc.unesco.org/en/list/121 [Accessed: 01 November 2017]

Unknown translator (1981). Brhatsamhit*ã*. 1st Edition. New Delhi: Motilal Banarsidass.

Von der Heide, S. (2017). After the earthquakes: Damaged ancient heritage sites in Mustang – challenges for renovation, restoration and reconstruction. Heritage at Risk: Pathways to the Protection and Rehabilitation of Cultural Heritage in South Asia. Kathmandu, 3 – 7 September 2017. Available: https://www.dur.ac.uk/cech/unescochair/workshops/heritageatrisk/

Weise, K. (2017). Preparing for the next earthquake: international standards for disaster risk management for cultural heritage. Heritage at Risk: Pathways to the Protection and Rehabilitation of Cultural Heritage in South Asia. Kathmandu, 3 – 7 September 2017. Available: https://www.dur.ac.uk/cech/unescochair/workshops/heritageatrisk/